# Uncovering the mechanisms of clinically-relevant altered antibiotic responses of *Staphylococcus aureus* under wound infection-mimetic conditions

Colin D. Rieger[1], Ali Molaeitabari[1], Tanya E. S. Dahms[1] and Omar M. El-Halfawy[1*]

[1] Department of Chemistry and Biochemistry, Faculty of Science, University of Regina, Regina, SK, S4S 0A2, Canada

[*] Correspondence: omar.el-halfawy@uregina.ca (O.M.E.)

**Running title:** Altered antibiotic responses of *S. aureus* under wound-like conditions

**Summary:**

Standard *in vitro* antimicrobial susceptibility testing (AST) using Mueller-Hinton broth (MHB) does not reflect infection-site conditions, and its results often do not correlate with therapeutic outcomes. Here, we compared the antibiotic susceptibility of methicillin-resistant *Staphylococcus aureus* (MRSA), a common chronic wound pathogen, in simulated wound fluid (SWF) resembling wound exudate versus MHB, revealing discordant AST results across six of nine tested antibiotic classes. The most significant were 128-fold increased resistance to tetracyclines and 256-fold sensitization to β-lactams in SWF. Tetracycline resistance was mediated by MntC, an extracellular manganese-binding protein, whereas β-lactam sensitization was driven by cell envelope remodelling in SWF. *Galleria mellonella* wound infection results matched the SWF susceptibility phenotypes, suggesting SWF better predicts *in vivo* wound infection therapeutic outcomes. These comprehensive phenotypic and mechanistic insights into MRSA antibiotic responses under wound-infection-mimetic conditions with direct *in vivo* validation identify a potential new antibiotic adjuvant target and may guide improved antibiotic therapy for MRSA wound infections.

## Introduction

Antibiotic resistance is rising at an alarming rate, and existing antibiotics are failing to treat infections [1]. This crisis further complicates chronic infections, which pose significant healthcare and socioeconomic challenges [2]. Chronic wounds are particularly troublesome because they have a prolonged inflammatory phase and delayed healing, leading to tissue fibrosis and non-healing ulcers [3,4]. Wound exudates produced during healing are serum-based fluid rich in protein and growth factors, providing a suitable environment for bacterial colonization [5]; such infections frequently fail to respond to treatment [3]. Chronic wound infections are estimated to affect 1-2% of the world population at some point in their lives [6]. Wound care poses a substantial economic burden on the healthcare system; wound care costs were estimated to be ~$300B worldwide in 2019 [7] – such expenditures in the 10 highest spending countries alone increased from ~$233B in 2019 to $301B in 2022 [8].

*Staphylococcus aureus,* a Gram-positive pathogen, is a leading cause of both hospital- and community-acquired infections worldwide, associated with bacteremia, endocarditis, skin and soft tissue infections (SSTIs), and other infections affecting almost all body sites [9-11]. Notably, *S. aureus* is the leading cause of SSTIs, including complicated SSTIs such as chronic wounds and burn infections **[11-13]**. If not treated, *S. aureus* wound infections can spread to bloodstream infections, which are often fatal **[14]**. *S. aureus* developed multi-drug resistance, including to last-resort antibiotics, placing it on the World Health Organization's list of 'priority pathogens' posing the greatest threat to human health [15]. Methicillin-resistant *S. aureus* (MRSA, known for resistance to β-lactam antibiotics) is the leading cause of wound infections, posing severe clinical problems [13]. Currently, the most commonly circulating community-associated MRSA lineage in North America is USA300 **[16]**. The discovery of new antibiotics has lagged

51 behind the constant rise in AMR prevalence [10]. There is an urgent need for new antimicrobial
52 solutions, including antibiotic adjuvants that revive currently failing antibiotics.

53 Bacterial antibiotic responses are often studied under standard *in vitro* conditions [e.g.,
54 Mueller-Hinton broth (MHB), composed of beef extract, casein hydrolysate, and starch[17]] that do
55 not adequately reflect the infection site. These assays, standardized by agencies such as CLSI[18],
56 are routinely used in clinical labs worldwide to determine whether a clinical isolate is sensitive
57 or resistant to an antibiotic, guiding antibiotic therapy. Nonetheless, the clinical outcome often
58 does not correlate with standard antibiotic susceptibility test (AST) results, with reports of
59 unexpected antibiotic therapeutic failure [19-21]. In contrast, unexpected potency in patients despite
60 AST-predicted resistance is far less frequently reported, as such antibiotics would typically be
61 contraindicated. However, anecdotal reports describe instances in which an antibiotic empirically
62 prescribed while waiting (up to 72 h) for AST results shows efficacy in patients before AST
63 identifies the causative isolate as resistant to the same antibiotic. Together, standard AST
64 erroneous predictions can lead to therapeutic failure or sideline much-needed *in vivo*-effective
65 antibiotics.

66 Culture conditions and media composition dictate gene expression and dispensability
67 profiles in bacteria to meet their survival requirements [22,23], thereby potentially altering bacterial
68 antibiotic responses. Infection-mimetic media, such as simulated wound fluid (SWF) [24], have
69 been developed, providing test conditions that are more clinically relevant than MHB for
70 assessing bacterial responses. SWF is composed of 50% v/v fetal bovine serum in maximal
71 recovery diluent, which is an isotonic peptone saline solution [24]. Such a formulation of SWF
72 mimics chronic wound exudates, as the latter are derived from serum and contain electrolytes at
73 concentrations equivalent to those in serum, approximately half the total protein content of

74 serum, and higher levels of growth factors for tissue regeneration [25-29]. The inclusion of fetal
75 bovine serum in this recipe provides additional components not present in MHB, such as growth
76 factors, transport proteins, enzymes, hormones, fatty acids, and lipids, at biologically relevant
77 levels [30,31].

78 Here, we used SWF to evaluate the antimicrobial susceptibility profile of MRSA under
79 wound infection-mimetic conditions. We observed discordance in AST results for representative
80 antibiotics across six of nine antibiotic classes tested in SWF compared to MHB against the
81 MRSA USA300. The antibiotic classes showing the most significant discordant AST results
82 included tetracyclines, to which USA300 was more resistant (up to a 128-fold shift), and β-
83 lactams, to which the MRSA was unexpectedly more sensitive (up to a 256-fold shift), when
84 tested in SWF. Interestingly, these antibiotic susceptibility shifts crossed the CLSI clinical
85 breakpoint for representatives of both classes, suggesting they may result in altered therapeutic
86 outcomes. Genome-wide assays and subsequent mechanistic characterizations revealed that the
87 increased resistance to tetracyclines is mediated by MntC, an extracellular binding protein of a
88 manganese ABC transporter system, whereas the drastic sensitization to β-lactams was driven by
89 cell envelope remodelling in SWF. Further, we used a *Galleria mellonella* incision wound
90 infection model, which shows wound healing events similar to those in animals [32] and
91 recapitulates the hallmarks of trauma and infection observed in mammalian models [33], to
92 characterize the observed *in vitro* phenotypes. Doxycycline, a tetracycline antibiotic, could not
93 rescue wild-type USA300-infected Galleria larvae but significantly increased the survival of
94 those infected with the *mntC*::Tn mutant, whereas the β-lactam cefuroxime was effective at
95 rescuing a significant number of USA300-infected larvae. These *in vivo* results matched the *in*

96 *vitro* phenotypes in SWF but not MHB, suggesting that this host-mimetic medium is a better
97 predictor of *in vivo* MRSA wound infection therapeutic outcomes.
98 Together, this work addresses the relatively long-recognized shortcomings of the MHB-
99 based standard AST by uncovering alterations in MRSA antibiotic susceptibility in wound
100 exudate-like fluid relative to MHB. Further, this study not only describes the phenotypic
101 differences between SWF and MHB but, more importantly, also systematically reveals the
102 specific molecular mechanisms underlying the most significant discordant AST results between
103 standard and infection-mimetic conditions at the whole-genome level, and directly links the
104 uncovered *in vitro* phenotypes and mechanisms to *in vivo* efficacy. Therefore, our results provide
105 a solid theoretical basis for improved antibiotic selection in the clinic and a potential new target
106 for adjuvant therapy against drug-resistant MRSA wound infections.
107
108 **Results:**
109 **Alterations in MRSA sensitivity to antibiotics in SWF.**
110 We first compared AST results of representative antibiotics from nine classes against
111 USA300 cultured in MHB and SWF (Table 1). Six of the nine classes showed discordance in
112 minimum inhibitory concentration (MIC) determined in the two media (MIC ≥ 4-fold difference
113 between SWF and MHB, Table 1). These MIC discordances included a 128-, 16-, and 4-fold
114 sensitization in SWF to azithromycin (a macrolide), colistin (a polymyxin antimicrobial peptide),
115 and daptomycin (a lipopeptide), respectively, and an 8-fold increase in rifampicin MIC in SWF
116 against USA300 (Table 1). These MIC shifts did not cross the CLSI breakpoints for the four
117 antibiotic classes in USA300 (Table 1). Yet, similar MIC fold shifts in other *S. aureus*
118 backgrounds that are less susceptible to these antibiotics may alter the predicted antibiotic

119 susceptibility, warranting future testing in other *S. aureus* lineages. The remaining two antibiotic
120 classes showing the most significant fold shift in MIC in SWF relative to MHB are tetracyclines
121 that showed an increase in MIC when tested in SWF (e.g., a 128-fold shift for tetracycline from
122 0.25 μg/mL in MHB to 32 μg/mL in SWF) and β-lactams that showed a decrease in MIC in SWF
123 (e.g., a 256-fold shift for cefuroxime from 1024 μg/mL in MHB to 4 μg/mL in SWF, Table 1).
124 Importantly, the MIC fold shifts crossed the CLSI clinical breakpoint for representatives of these
125 two classes (Table 1). Together, we chose to focus on these two classes to uncover the
126 mechanism underlying the observed altered antibiotic susceptibility under the wound-mimetic
127 condition.

128 Tetracycline antibiotics inhibit protein synthesis by binding to the 30S ribosome subunit
129 [34]. Doxycycline is a second-generation tetracycline that showed a 32-fold increase in MIC
130 against USA300 from 0.125 μg/mL in MHB to 4 μg/mL in SWF (Table 1). In addition, we
131 assessed the third-generation tetracycline, omadacycline, and found that its MIC against USA300
132 doubled in SWF relative to MHB (Table 1). These results demonstrate that the increased
133 resistance in SWF is conserved across the three generations of tetracyclines. Doxycycline is
134 more clinically relevant than tetracycline for treating MRSA skin and soft tissue infections
135 (SSTIs) [35]; therefore, we used it as a representative of this class in the remainder of this study. On
136 the other hand, cefuroxime is a β-lactam antibiotic that binds to penicillin-binding protein 2,
137 inhibiting bacterial cell wall synthesis [36]. Oxacillin, another β-lactam, is used by CLSI to
138 distinguish MRSA from methicillin-sensitive *S. aureus* (MSSA) [18]; it showed a 64-fold decrease
139 in MIC against USA300 in SWF (from 64 μg/mL in MHB to 1 μg/mL in SWF), bringing the
140 MIC below the CLSI MRSA breakpoint (Table 1). We initially tested both β-lactams and then
141 focused on cefuroxime for subsequent mechanistic testing.

142 To determine how conserved the doxycycline and β-lactam susceptibility alterations in
143 SWF are across multiple MRSA strains, we determined the MICs of antibiotics against a panel of
144 isolates representing the most commonly circulating lineages of MRSA in Canada [CMRSA
145 strains [37]] in both MHB and SWF. All CMRSA strains showed increased resistance (≥ 8-fold
146 shift in MIC) to doxycycline when tested in SWF relative to MHB (Table 2). All CMRSA strains
147 exhibited increased sensitivity to both β-lactams in SWF, except for CMRSA 1 and CMRSA 4,
148 with MIC shifts in CMRSA 5, 7, 8, and 10 crossing the CLSI breakpoint for one or both
149 antibiotics (Table 2). Given the magnitude of antibiotic susceptibility alterations conserved
150 across strains from multiple MRSA lineages, we next sought to determine the mechanisms of
151 doxycycline and cefuroxime susceptibility alterations in the wound-mimetic medium in MRSA
152 using USA300 as a representative being one of the most common community-associated MRSA
153 strains.
154
155 **A chemogenomic screen to uncover the mechanism of increased resistance to doxycycline in**
156 **SWF.**
157 To investigate the increased resistance of USA300 to doxycycline when cultured in SWF,
158 we screened the Nebraska Transposon Mutant Library (NTML), a sequence-defined transposon
159 insertion library comprising 1920 mutants that cover the non-essential genome of USA300 [38], at
160 supra-inhibitory (in MHB) and sub-inhibitory (in SWF) concentrations of doxycycline. The
161 NTML supra-inhibitory screen in MHB (at 1 µg/mL doxycycline, 8X the MIC in MHB), which
162 aimed to identify putative sensitivity determinants, and follow-up dose-response assays did not
163 reveal any mutants more resistant to doxycycline in MHB relative to the wild-type (Fig. S1A-C).
164 On the other hand, the NTML sub-inhibitory screen in SWF (at 0.125 µg/mL doxycycline, 1/32$^{nd}$

165 the MIC in SWF), which aimed to identify putative determinants of doxycycline resistance, and
166 follow-up MIC assays revealed that *mntB*::Tn and *mntC*::Tn were sensitive to doxycycline in
167 SWF relative to USA300 (Fig. 1A-C and Fig. S2). To verify the observed phenotypes, we
168 genetically complemented *mntB* and *mntC* in their transposon mutants. While *mntC*
169 complementation restored doxycycline resistance of *mntC*::Tn, *mntB* alone was not sufficient to
170 restore doxycycline resistance in *mntB*::Tn, but rather both *mntB* and *mntC* were required (Fig.
171 S3A-C). As such, the *mntB*::Tn phenotype may be due to polar effects from the transposon
172 insertion into *mntB,* disrupting the downstream *mntC* (Fig. S3C). Together, this work identifies
173 MntC as the determinant of increased doxycycline resistance in the wound-like medium.
174
175 **MntC increases doxycycline resistance in wound-like medium.**
176 Next, we set out to determine the mechanism by which MntC increases doxycycline
177 resistance in SWF. MntABC, an ABC transporter that imports manganese, is comprised of an
178 ATP-binding protein (MntA), a transmembrane protein (MntB), and an extracellular binding
179 protein (MntC) [39]**;** therefore, we initially hypothesized that manganese or other divalent cations
180 imported by MntC contributed to the increased resistance to doxycycline. However, exogenously
181 supplementing manganese, calcium, magnesium, cobalt, iron, copper, and zinc, in dose-
182 dependent checkerboard assays with doxycycline against wild-type USA300 and *mntC*::Tn in
183 MHB did not alter the susceptibility to doxycycline except for iron, which showed antagonism in
184 both strains suggesting the observed iron effect is MntC-independent (Fig. S4). Conversely,
185 higher concentrations of manganese antagonized doxycycline in SWF both in the wild-type and
186 the *mntC* mutant (FICI = 6.75 and 32.5, respectively; Fig. S5). Such effect might be due to
187 compensation of the sequestration of manganese in SWF due to chelators, such as calprotectin,

188 likely present in fetal bovine serum. Together, manganese and other divalent cations appear to
189 play no role in the MntC-mediated doxycycline resistance observed in SWF.
190 Next, we hypothesized that MntC sequesters doxycycline, lowering its intracellular
191 concentration, thereby increasing resistance to that antibiotic in bacteria cultured in SWF. To
192 address this hypothesis, we first determined the intracellular concentration of doxycycline in
193 *mntC*::Tn relative to the wild-type cultured in MHB and SWF. In SWF, *mntC*::Tn had a greater
194 intracellular concentration of doxycycline relative to USA300, whereas both the wild-type and
195 mutant strains showed similar intracellular doxycycline content in MHB (Fig. 1D), aligning with
196 our previous results showing a SWF-specific role of MntC in doxycycline resistance and
197 supporting our hypothesis of a potential sequestration of doxycycline by MntC. Next, we
198 assessed the ability of purified recombinant MntC to bind doxycycline using a fluorescent
199 binding assay conducted in HEPES buffer in which doxycycline fluorescence increased upon
200 binding to a ligand. Using bovine serum albumin and lysozyme as positive [40] and negative
201 controls, respectively, in this assay, we revealed that MntC binds doxycycline (Fig. 1E), which
202 likely reduces its intracellular concentration (Fig. 1D). Given that such a binding interaction does
203 not require any component of SWF, as it occurred in HEPES buffer, we posited that MntC-
204 mediated increased doxycycline resistance occurs in SWF only due to an upregulation of *mntC*
205 under wound-like conditions. Hence, we assessed the transcriptional differences in *mntC* using
206 qRT-PCR. We revealed that *mntC* was upregulated by ~20-fold in wild-type USA300 cultured in
207 SWF relative to MHB, irrespective of doxycycline treatment (Fig. 1F), demonstrating that the
208 *mntC* upregulation is induced by the wound-like culture condition rather than a specific response
209 to doxycycline. In fact, doxycycline exposure downregulated *mntC* in USA300 in both SWF and
210 MHB to a similar extent (~4-fold; Fig. S6). In summary, the increase in doxycycline resistance in

211 the wound-like medium is due to an upregulation of *mntC*, whereby the overexpressed MntC can
212 sequester doxycycline, decreasing its effective intracellular concentration.
213
214 **MntC contributes to doxycycline resistance *in vivo* in a *Galleria mellonella* wound infection**
215 **model.**
216 Next, we sought to assess whether MntC contributed to doxycycline resistance *in vivo* in
217 a wound infection model. To that end, we tested the *mntC*::Tn mutant in a *Galleria mellonella*
218 incision wound infection model. Galleria mounts both cellular and humoral innate immune
219 responses closely resembling those of vertebrates and thrives at mammalian body temperature
220 [41,42]. Incision wounds have been histologically characterized in Galleria larvae, showing wound
221 healing events similar to those in animals [32], and their wound model recapitulates the hallmarks
222 of trauma and infection observed in mammalian models [33]. Infection with either the wild-type
223 USA300 or the *mntC*::Tn mutant, both treated with the vehicle control (Glaxal™ Base non-
224 medicated cream), led to 100% larval fatality by the end of the experiment (at 6 days); however,
225 we observed a significant increase in survival of larvae infected with *mntC*::Tn relative to
226 USA300 at day 1 (Fig. 1G), suggesting a role of MntC in virulence. Further, a single dose of
227 doxycycline treatment (4 μL of 10% w/w cream, i.e., 0.4 mg/incision) increased survival of
228 *mntC*::Tn-infected larvae to 45% compared to only 7.5% survival in wild-type-infected ones
229 (Fig. 1G). Together, knocking out *mntC* increased the sensitivity of USA300 to doxycycline *in*
230 *vivo,* consistent with the *in vitro* SWF phenotype, demonstrating that MntC is a potential target
231 for doxycycline adjuvant therapy for MRSA wound infections.
232

233 **A chemogenomic screen to uncover the mechanism of MRSA susceptibility to β-lactams in**
234 **SWF.**

235 To investigate the increased sensitivity of USA300 to cefuroxime in SWF, we screened
236 the NTML in SWF at 16 µg/mL of cefuroxime (4X the wild-type MIC in SWF) to identify
237 susceptibility determinants. However, none of the mutants with greater than 25% relative growth
238 at this supra-inhibitory concentration in SWF showed increased cefuroxime MIC in follow-up
239 MIC assays (Fig. S7A-C). We also screened the NTML in MHB at 128 µg/mL of cefuroxime
240 (1/8$^{th}$ the wild-type MIC in MHB) to identify putative determinants of cefuroxime resistance,
241 revealing 101 mutants with <8% growth at this sub-inhibitory concentration relative to their
242 untreated controls (Fig. 2A-B). We hypothesized that mutants of determinants underlying
243 cefuroxime sensitivity in SWF would be susceptible to cefuroxime in MHB, with no further
244 sensitization in SWF relative to the parent strain. To that end, we tested the 101 mutants in dose-
245 response and MIC assays. Nine mutants showed ~128 to 256-fold sensitization to cefuroxime
246 relative to the parent strain in MHB (i.e., showing MICs similar to or within 2-fold of that of
247 USA300 in SWF) with relatively minimal MIC reduction relative to USA300 (≤4-fold) in SWF,
248 revealing putative primary determinants of this phenotype (Fig. 2C). An additional 12 mutants
249 showed a relatively more modest shift in cefuroxime MIC in MHB, potentially identifying
250 secondary determinants of the phenotype (Fig. S8).

251 Six of the primary determinants (Fig. 2C) are localized to or involved in cell envelope
252 homeostasis; their gene products are related to peptidoglycan synthesis [*pbp2a* and *pbp4*,
253 encoding penicillin binding proteins (PBPs)], wall teichoic acid [WTA; *tcaA* and *fmtA*], and cell
254 envelope stress response [*graR* and *vraF,* encoding members of the GraXSR-VraFG five-
255 component response system] [43-47]. Interestingly, some of the secondary determinants (Fig. S8)

256 are involved in similar processes [MurA2, predicted to be involved in biosynthesis and
257 degradation of peptidoglycan; RsbU and RsbV, involved in the regulatory cascade of the master
258 transcriptional regulator $\sigma^B$ that provides protection from stress and influences cell envelope
259 composition [48]] or localize at the membrane [SAUSA300_2297, SAUSA300_0073,
260 SAUSA300_1785, SAUSA300_1484, SAUSA300_2315, and SpsA; predictions from [49]]. The
261 genes encoding the remaining three primary determinants are SAUSA300_0794 (encodes a
262 TOPRIM domain-containing protein previously shown to be hypersensitive to the β-lactam
263 amoxicillin [50]), *aapA* (encodes a D-serine/D-alanine/glycine transporter), and *yabJ* (encodes a
264 putative endo-RNase L-PSP). Importantly, most of the primary cell envelope-related
265 determinants (Fig. 2C) are genetically interconnected as shown in synthetic lethal interaction
266 analyses [51]. Given that most mutants identified above harbour disruptions related to the cell
267 envelope, which also comprises the β-lactam target (peptidoglycan), we then set out to
268 characterize the primary cell envelope-related determinants and assess their implications for the
269 unexpected β-lactam hypersensitivity of the MRSA USA300 in the wound-like medium.
270

271 **Decreased abundance of penicillin-binding proteins (PBPs) contributes to cefuroxime**
272 **susceptibility in SWF.**

273 First, we investigated the potential role of alterations in PBPs in the SWF-specific
274 cefuroxime susceptibility phenotype, especially given that PBPs are the main targets of β-
275 lactams and that the primary resistance mechanism of MRSA is the low-affinity alternative
276 PBP2a encoded by *pbp2a* or *mecA* [52]. Based on *pbp2a*::Tn and *pbp4*::Tn cefuroxime
277 susceptibility phenotypes (Fig. 2C), we hypothesized that USA300 cultured in SWF would have
278 decreased abundance of these PBPs. To directly assess the abundance of PBPs in USA300, we

279 isolated membrane fractions from cultures grown in MHB and SWF and then used a fluorescent
280 penicillin (BOCILLIN™ FL) to bind and detect PBPs resolved on SDS-PAGE. Quantification of
281 band density identified a ~25, ~21, and ~55 percent reduction in the relative abundance of PBP1,
282 2, and 4, respectively, in SWF compared to MHB (Fig. 3A, Fig. S9A, B). Notably, PBP1 and
283 PBP2 are essential genes and therefore are not in the NTML [46]. Also, BOCILLIN™ FL labels all
284 PBPs except PBP2a due to its decreased affinity for penicillin. Therefore, we assessed PBP2a
285 abundance by Western blot using an anti-PBP2a-specific antibody [53], revealing a ~20 percent
286 decrease in the relative abundance of PBP2a in USA300 cultured in SWF relative to MHB (Fig.
287 3B, Fig. S9C, D). Together, the decreased abundance of the four PBPs (1, 2, 2a, and 4) in SWF is
288 likely a major contributor to the decreased β-lactam susceptibility of USA300 under the wound-
289 like condition.
290
291 **Wall teichoic acid alterations contribute to USA300 sensitivity to cefuroxime in SWF.**
292 Next, we sought to evaluate changes in WTA, which plays a role in the coordination of
293 peptidoglycan synthesis and β-lactam resistance [54,55]. First, we sought to test *tarO,* which
294 encodes a *N*-acetylglucosamine-1-phosphate transferase, the first committed step in WTA
295 production [56]. A *tarO* knockout is not within the NTML, and thus was not tested in our screen. A
296 CMRSA10Δ*tarO* was ≥256-fold more susceptible to cefuroxime in MHB but only ~4-fold more
297 susceptible to the β-lactam in SWF relative to the wildtype (Fig. 3C), mirroring the phenotype of
298 the primary determinants identified above (Fig. 2C). We then used targocil, an inhibitor of the
299 WTA flippase TarG [57], to determine if culturing in SWF disrupts TarO or WTA biosynthesis.
300 While targocil is lethal, knocking out genes encoding early steps in the WTA synthesis pathway
301 (*tarO* and *tarA*) or inhibiting their products, which completely block WTA biosynthesis,

302 antagonizes targocil [58]. We observed an ~8-fold increase in targocil MIC against wildtype
303 USA300 when tested in SWF relative to MHB, raising the MIC up to 32 μg/mL (Fig. 3C). In
304 comparison, the targocil MIC against the Δ*tarO* mutant was >64 μg/mL in both media (Fig. 3C),
305 which together suggests that WTA biosynthesis is at least partially disrupted in SWF.

306 TarO inhibition has been associated with the delocalization of PBP2, leading to increased
307 β-lactam sensitivity [59]. Epicatechin gallate (ECg) induces partial delocalization of PBP2 from the
308 division septum, mimicking the effects of TarO inhibition [59]. As expected, ECg synergized with
309 cefuroxime against the wild-type USA300 in MHB (FICI = 0.023 ± 0.005; Fig. 3D). However,
310 such synergy was lost when we tested the same combination in SWF (FICI = 2.2 ± 0.2; Fig. 3D),
311 suggesting PBP2 was already delocalized, potentially due to WTA biosynthesis disruption, under
312 the wound-like condition.

313 Next, we directly evaluated the abundance of WTA in SWF and MHB (Fig. 3E-G, Fig.
314 S10A). We tested both the wild-type USA300 strain and the *tcaA*::Tn mutant identified from the
315 screen (Fig. 2), as *tcaA* encodes a teicoplanin resistance-associated protein involved in WTA
316 retention and robustness of *S. aureus* peptidoglycan crosslinking [43]. USA300 cultured in SWF
317 showed a significant decrease in WTA abundance relative to MHB (Fig. 3E, F). The WTA
318 abundance of the wild-type grown in SWF was comparable to that observed in the *tcaA*::Tn
319 mutant cultured in MHB or SWF (Fig. 3E; no significant difference across these three
320 conditions). Notably, the WTA bands from the wild-type cultured in SWF migrated slightly
321 further on the PAGE relative to those from an MHB culture (Fig. 3F, G), suggesting a shorter
322 WTA polymer. However, the shorter polymer length was not associated with TcaA, as the same
323 occurred in the *tcaA*::Tn mutant (Fig. 3F, G).

324 WTA, its influence on PBP localization, and gene products associated with that polymer,
325 such as FmtA (a teichoic acid D-Ala esterase) and TcaA, are involved in the structural integrity
326 of the cell envelope, which can alter the bacterial autolysis [43,44,60]. Therefore, we assessed the
327 0.02% Triton X-100-induced lysis of USA300, relative to knockouts of *fmtA* and *tcaA,* in MHB
328 and SWF. Wild-type USA300 cells harvested from SWF cultures showed significantly faster
329 Triton-induced lysis rates relative to those from MHB cultures (Fig. 3H, I, Fig. S10B-D). There
330 was no further increase in lysis rates in SWF due to disrupting *tcaA* and *fmtA,* where both
331 mutants showed no statistical difference in lysis rate compared to the wild-type cultured in SWF
332 (Fig. 3H, I, Fig. S10B-D), suggesting WTA-associated gene products may have already been
333 disrupted in SWF. In all cases, these observations are consistent with the alterations in WTA and
334 PBP localization observed in SWF.
335 Next, we indirectly assessed cell surface charge, which is partly influenced by WTA
336 retention, by quantifying binding to cytochrome c, a highly positively charged protein. A
337 decreased abundance of WTA, a polyribitol phosphate polymer that generally imparts a strong
338 negative charge to the surface [61], should reduce the overall net negative charge of the cell
339 surface. USA300 cultured in SWF showed a significant decrease in binding to cytochrome c
340 compared with MHB (Fig. 3J). We observed a decrease in relative cytochrome c binding to
341 *tcaA*::Tn compared to that of USA300, but no difference in cytochrome c binding between
342 *tcaA*::Tn cultured in MHB and SWF (Fig. 3J). These results align with the respective relative
343 WTA abundance (Fig. 3E). Of note, other factors can also influence surface charge, such as
344 MprF, a phosphatidylglycerol lysyltransferase, which decreases the net negative charge of the
345 cell surface through lysyl modification of the cytoplasmic membrane, conferring resistance to
346 cationic antimicrobials [62]. While the cytochrome c binding of *mprF::Tn* in SWF relative to MHB

347 followed the same trend observed for the wild-type strain, the lack of such modification in
348 *mprF*::Tn increased the binding to cytochrome c relative to wild-type USA300 in each of the
349 tested media, as expected (Fig. 3J). Taken together, the results in this section demonstrate WTA-
350 related alterations that may contribute to the increased β-lactam susceptibility of the MRSA
351 USA300 in the wound-mimetic medium.
352
353 **A lack of antibiotic-mediated induction of the GraXSR VraFG system in SWF.**
354 GraXSR VraFG is a five-component system that regulates the bacterial response to cell
355 envelope stress, such as exposure to cationic antimicrobial peptides, through processes that
356 include the DltABCD-mediated D-alanylation of teichoic acids and the MprF-dependent
357 lysylination of phosphatidylglycerol [63]. Notably, disruptions of GraR sensitize MRSA to β-
358 lactams [58]. *mprF* is positively regulated by GraXSR, and the system is strongly induced by
359 colistin, a cationic antimicrobial peptide [58]. Hence, we assessed the colistin-mediated induction
360 of the GraXSR VraFG system in SWF compared to tryptic soy broth (TSB), a standard culture
361 medium, by monitoring luciferase reporter expression under the control of the *mprF* promoter.
362 As previously reported [58], we observed a colistin-mediated *graR*-dependent induction of the
363 *mprF* promoter in TSB, where there was a significant increase in luciferase signal in the presence
364 of colistin in the wild-type (Fig. 4A) but not in the Δ*graR* mutant (Fig. S11A-C). Such colistin-
365 mediated *mprF* promoter induction was not observed in SWF (Fig. 4A); instead, a significant
366 *graR*-independent repression of the *mprF* promoter at 3 hours by colistin was observed in both
367 the wild-type (Fig. 4A) and the Δ*graR* mutant (Fig. S11D-F). To further assess the role of the
368 GraXSR VraFG system in antibiotic response in SWF, we used MAC-545496, a GraR inhibitor
369 previously shown to synergize with β-lactams in MHB [58]. As expected, we observed a *graR*-

370 dependent synergy between MAC-545496 and cefuroxime against USA300 in MHB (FICI =
371 0.036 ± 0.014; Fig. 4B; not observed against *graR*::Tn, FICI = 1.04 ± 0.47; Fig. S12). Such
372 synergy was lost in SWF (FICI = 2.0 ± 0.0; Fig. 4B). Together, the lack of *mprF* promoter
373 induction by colistin and loss of MAC-545496-cefuroxime synergy in SWF illustrate the lack of
374 stress-mediated induction of GraR and its regulon, and hence the disruption of the GraXSR
375 VraFG cell envelope stress response system, in the simulated wound fluid. Notably, such
376 alteration in cell envelope stress response (Fig. 4) along with changes in cell envelope structures
377 (the decreased abundance of several penicillin-binding proteins and wall teichoic acid; Fig. 3) of
378 the MRSA USA300 under wound-like conditions can collectively result in the β-lactam
379 sensitivity of MRSA in SWF (See Discussion Section and Fig. 7B).
380
381 **Ultrastructural, biochemical, and mechanical changes to USA300 grown in SWF.**
382 Next, we further assessed the cell and its envelope using atomic force microscopy (AFM)
383 to compare cell size, surface topography, roughness, elasticity, and adhesion. We observed a
384 significant increase in cell size (height and diameter) and surface roughness of USA300 cultured
385 in SWF relative to that cultured in MHB (Fig. 5A-H, Fig. S13, 14). The surface of USA300 cells
386 harvested from SWF culture was more compliant relative to those from MHB, requiring less
387 force to deform (Fig. 5I). Adhesion values between the negatively charged silicon nitride AFM
388 tip and the cell surface were greater for USA300 cells cultured in SWF relative to MHB (Fig.
389 5J), consistent with the cytochrome c binding assays showing that USA300 cultured in SWF are
390 less negative than those in MHB (Fig. 3J). Together, these results provide further evidence for
391 cell envelope-related alterations in simulated wound fluid, which underpins the increased β-
392 lactam susceptibility.
393

394 **Cefuroxime rescues USA300-infected Galleria larvae.**

395 Next, we sought to determine the efficacy of cefuroxime against USA300 in an *in vivo G.*
396 *mellonella* incision wound infection model. Infection with wild-type USA300 treated with the
397 vehicle control (Glaxal$^{TM}$ base non-medicated cream), led to only 10% and 2.5% larval survival
398 by days 3 and 6 post-infection, respectively (Fig.6). In contrast, a single dose cefuroxime
399 treatment (4 μL of 40% w/w cream, i.e., 1.6 mg/incision) significantly increased the survival of
400 USA300-infected larvae to ~75% and 45% at the same timepoints post-infection ($p<0.0001$; Fig.
401 6). Together, the efficacy of cefuroxime against USA300 *in vivo* aligns with the *in vitro*
402 susceptibility to that β-lactam antibiotic in SWF, demonstrating that this wound exudate-mimetic
403 medium may be superior to MHB for predicting clinical outcomes of MRSA wound infections.
404

405 **Discussion**

406 Standard MHB-based AST assays have been widely used worldwide to guide
407 antimicrobial therapy and study antimicrobial resistance. However, MHB does not accurately
408 reflect the conditions at the site of infection [64], and the clinical outcome often does not correlate
409 with standard AST results [19-21]. Further, antibiotic discovery has traditionally relied on standard
410 AST conditions, partly because of regulatory requirements to demonstrate efficacy under such
411 conditions for approval [65], which has likely limited the suite of potential antimicrobial targets
412 and bioactives. Therefore, there are emerging efforts to study bacterial responses and screen for
413 new antimicrobials under infection-relevant conditions to bridge the gap between *in vitro* testing
414 and *in vivo* outcomes [E.g., [43,66-70]]. Herein, we studied the antibiotic responses of MRSA under
415 wound-infection-mimetic conditions, revealing ~67% discordance in AST results between
416 simulated wound fluid and MHB. Similar discordances were observed in analyses using serum-
417 containing and other eukaryotic cell culture media (e.g., RPMI) [71,72]. We then sought to elucidate

418 the mechanisms underlying the two most significant antibiotic susceptibility alterations in the
419 MRSA USA300 strain in terms of fold-shift and potential clinical relevance, the unexpected
420 resistance to tetracyclines and sensitization to β-lactams in SWF.

421 We revealed that the unexpected increase in resistance to first-, second-, and third-
422 generation tetracyclines under wound-like conditions is mediated by MntC (Fig. 7A). MntC has
423 not been previously known to confer tetracycline resistance, a role overlooked in standard culture
424 conditions but detected in SWF. We observed an upregulation of *mntC* in SWF relative to MHB,
425 independent of tetracycline exposure, suggesting MntC expression is induced by the culture
426 condition rather than the antibiotic. Interestingly, the observed unexpected resistance to
427 tetracyclines appears to corroborate reports of therapeutic failures with tigecycline (a tetracycline
428 derivative) in soft-tissue, bloodstream, and other infections despite predicted efficacy [73,74]. Also,
429 the upregulation of *mntC*, which is highly conserved among *S. aureus*, in the serum-based SWF
430 aligns with observations from *in vivo* studies and patient samples [75-78]. MntC was only expressed
431 *in vivo* or in the presence of serum, and rapidly upregulated in *S. aureus* murine infection [75,76].
432 Anti-MntC antibodies protected against *S. aureus* in an infant rat model, and MntC could induce
433 a protective immune response; hence, it was identified as a potential vaccine target [75,76]. *mntC*
434 (also referred to as *sitA*) had increased transcription in three healthy persistently colonized
435 volunteers relative to *in vitro* conditions [77] and ranked among the first quartile of upregulated
436 genes in pediatric skin and soft tissue infection (SSTI) and murine SSTI abscesses [78]. As such,
437 unexpected clinical failures of tetracyclines against MRSA may occur due to MntC
438 overexpression *in vivo*. These observations, along with the increased survival of *mntC*::Tn-
439 wound infected Galleria larvae, relative to wild-type, upon treatment with doxycycline (Fig. 1G),
440 support that MntC could serve as an *in vivo*, clinically relevant drug target for new antibiotic

441 adjuvants for tetracyclines. Interestingly, infection with an *mntC* knockout increased animal
442 survival in a murine sepsis model, which was attributed to an increased susceptibility of the
443 mutant to oxidative stress [79], aligning with the increased larval survival at day 1 post-infection
444 with *mntC*::Tn relative to USA300 without treatment (Fig. 1G). These observations suggest that
445 MntC may also serve as a target for stand-alone anti-virulence therapy.

446 MRSA are characterized by their resistance to β-lactam antibiotics. As such, the
447 significant sensitization of tested MRSA strains from widely circulating lineages to
448 representative β-lactams in the simulated wound fluid is counterintuitive but suggests that β-
449 lactams may be a viable therapy for MRSA wound infections. *In vivo* results from the Galleria
450 incision wound infection model aligned with the *in vitro* data, whereby the β-lactam cefuroxime
451 improved the survival of MRSA USA300-infected larvae (Fig. 6). Interestingly, an observational
452 study of 2096 pediatric skin and soft tissue infection patients at a community-acquired MRSA-
453 endemic region in Philadelphia reported a therapeutic success of empiric β-lactam monotherapy
454 comparable or even superior to that of MRSA-active antibiotics [80], suggesting that β-lactams
455 likely cleared at least some MRSA infections, a regimen that standard AST would have
456 contraindicated. Further, other recent reports have shown that adding β-lactams to the empirical
457 therapy regimen improved bacterial clearance in MRSA bacteremia [81-84]. Mechanistically, we
458 revealed that cell envelope remodelling of the MRSA USA300 under wound-like conditions,
459 involving a decreased abundance of penicillin binding proteins PBP1, 2, 2a, 4 and wall teichoic
460 acid, along with a lack of antibiotic-mediated GraXSR VraFG induction (Fig. 7B), underpins the
461 sensitivity of MRSA to β-lactams in SWF. Notably, various cell envelope changes were
462 previously reported for *S. aureus* cultured in serum-containing media, altering responses to cell
463 wall-targeting and membrane-active antibiotics [43,66]. Together, our results and previous

464 observations suggest that MHB-based AST may erroneously exclude β-lactams from therapeutic
465 regimens, and that the wound exudate-like medium may be better than MHB at predicting β-
466 lactam antibiotic efficacy. β-lactams are broad-spectrum, well-tolerated antibiotics that offer oral
467 options [85]; hence, accurately predicting their potency and recommending their use when possible
468 would be valuable in the clinic.

469 Overall, host-mimetic media, such as SWF, may better predict bacterial resistance and
470 correlate more closely with positive clinical outcomes. Uncovering antimicrobial susceptibility
471 profiles discordant between infection-relevant (e.g., SWF) and standard (e.g., MHB) culture
472 media may enhance our understanding of antibiotic therapeutic responses during infection. By
473 revealing the mechanisms underlying the discordant phenotypes, we identified MntC as a
474 potential target for new antimicrobials that may reverse resistance to currently available
475 tetracycline antibiotics or suppress virulence *in vivo*. The phenotypes uncovered herein provide
476 an *in vitro* screening platform in SWF for therapeutics targeting MntC. Notably, we have recently
477 uncovered several natural bioactives that target MRSA planktonic and biofilm cells in simulated
478 wound fluid, but not in standard media[86], providing proof of concept for adjuvant discovery in
479 SWF. Our AST results in the wound-like medium could also guide and optimize the use of
480 currently available antibiotics.

481

482 **Limitations of the study:**

483 The *in vitro* AST and mechanistic studies under wound infection-mimetic conditions were
484 conducted in the FBS-containing SWF[24], which, while more representative of the wound
485 exudates than MHB, may still miss some host-relevant components, some of which may be
486 patient-specific, and lack the dynamic changes in composition and concentration that occur

487 throughout the phases of wound healing. Importantly, wound exudates may vary in appearance
488 and composition based on the etiology and specific conditions of the wound[25,87]. Hence, future
489 testing in other simulated wound fluids[88,89] with relatively minor compositional differences,
490 potentially reflecting variations across patient groups and healing phases, may be complementary
491 to this work. Additionally, the specific cues in SWF, representing potential host factors at wound
492 sites (such as extracellular matrix and coagulation cascade components, including fibronectin,
493 plasminogen, and fibrinogen that also bind to MntC[90], metal ion availability, or other factors),
494 and bacterial signalling pathways linking wound exudate microenvironmental exposure to
495 cellular responses, including MntC upregulation and the coordinated cell envelope remodelling,
496 are yet to be characterized, requiring further elucidation. Further, neither the *mntC*::Tn mutant
497 nor the *mntB*::Tn mutant, with both *mntB* and *mntC* disrupted (Fig. S3C), fully accounted for the
498 doxycycline MIC fold shift between MHB and SWF (Fig. 1A); a component of SWF inhibiting
499 tetracyclines may have contributed to the unaccounted-for ~2-fold increase in doxycycline MIC.
500 The most significant antibiotic susceptibility phenotypes and the role of MntC in resistance to
501 tetracyclines were tested *in vivo* in *G. mellonella*. While Galleria larvae mount both cellular and
502 humoral innate immune responses closely resembling those of vertebrates [41,42] and their wound
503 model recapitulates the hallmarks of trauma and infection observed in mammalian models [32,33],
504 their immune system and surface tissues still differ from those of mammals. Thus, future studies
505 should validate these Galleria results in *ex vivo* human skin and *in vivo* mammalian wound
506 infection models.
507
508 **Resource availability:**
509 **Lead contact**

- Further inquiries and requests should be directed to the lead contact, Omar El-Halfawy (omar.el-halfawy@uregina.ca).

**Materials availability**

- All reagents will be available upon request to the lead contact.

**Data and code availability**

- All data reported in this study are available in the Main and Supplemental Tables and Figures included in this publication.
- This paper does not report original code.
- Any additional information required to reanalyze the data reported in this paper is available from the lead contact upon request.

**Acknowledgements**:

This work was funded by a New Frontiers in Research Funds exploration grant (NFRFE-2021-00398), a Saskatchewan Health Research Foundation establishment grant (6115), a Canadian Institutes of Health Research grant (202403PPE-522800), Canada Foundation for Innovation and Innovation Saskatchewan grants, and start-up funds from the Faculty of Science at the University of Regina to O.M.E. O.M.E. holds a Canada Research Chair in Chemogenomics and Antimicrobial Research (CRC-2024-00304). C.D.R. was supported by a Canadian Institutes of Health Research Canada Graduate Scholarship – Master's (CGS-M) award. Work in the T.E.S.D. laboratory was supported by Natural Science and Engineering Research Council (NSERC DG 2024-06684) and Canada Foundation for Innovation grants to T.E.S.D. The Faculty of Graduate Studies and Research at the University of Regina provided partial support to A.M.

**Author contributions:**

Conceptualization: C.D.R., and O.M.E.; Formal analysis: C.D.R., and O.M.E.; Funding acquisition: O.M.E.; Investigation: C.D.R. and A.M.; Methodology: C.D.R., A.M., T.E.S.D., and O.M.E.; Project administration: O.M.E.; Resources: T.E.S.D. and O.M.E.; Supervision: T.E.S.D. and O.M.E.; Writing – original draft: C.D.R., and O.M.E.; Writing – review & editing: C.D.R., A.M., T.E.S.D., and O.M.E.

**Declaration of interests:**

The authors declare no competing interests.

**Supplemental information**

Document S1. Tables S1 and S2, Figures S1-S14, and supplemental references.

547 **Figure**

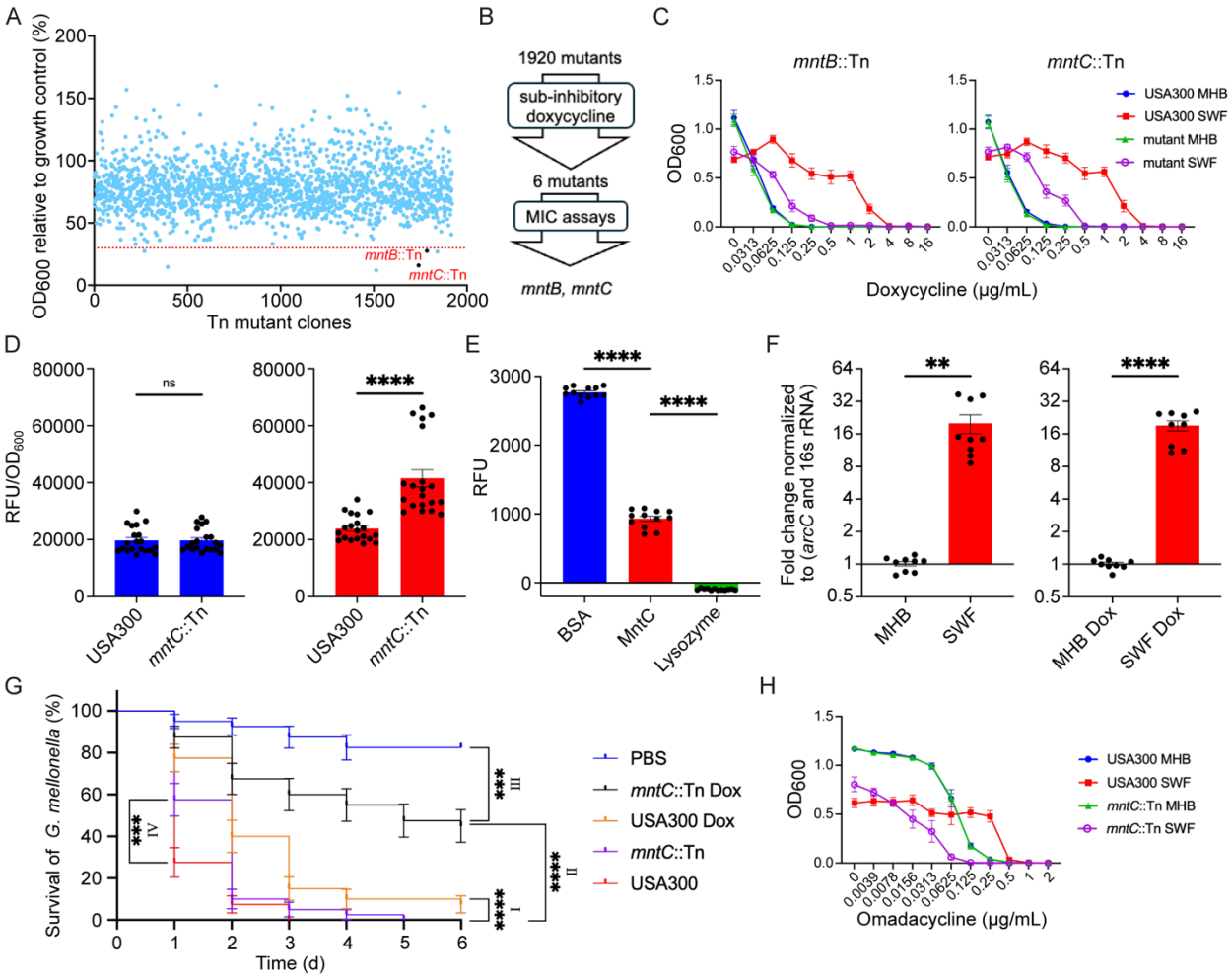


548

549 **Fig. 1 | MntC increases USA300 resistance to doxycycline in SWF**

550 A) A chemogenomic screen of the Nebraska Transposon Mutant Library with doxycycline at

551 1/32$^{th}$ the MIC in SWF. B) Workflow of the chemogenomic screen and follow-up assays that lead

552 to the putative determinants of doxycycline resistance. C) MIC assays of determinants of

553 USA300 doxycycline resistance in SWF. n = 9 from three independent experiments, shown as

554 mean ± SEM. D) Intracellular fluorescence of doxycycline relative fluorescent units

555 (RLU)/$OD_{600}$ in USA300 and *mntC*::Tn cultured in MHB (blue) or SWF (red). n = 20 from 4

556 independent experiments. E) Doxycycline binding assay in HEPES buffer showing increased

557 background-subtracted RFU upon doxycycline binding with the ligands bovine serum albumin

558 (positive control), MntC, and lysozyme (negative control). n = 12. F) Fold change in *mntC*
559 transcription from USA300 in SWF and MHB with or without doxycycline (relative to averaged
560 signals in MHB). n = 9 from three independent experiments. G) Kaplan-Meier survival curve of
561 *G. mellonella* treated with doxycycline or vehicle control, shown as mean ± SE. n = 40 from 4
562 independent experiments. H) MIC assays of omadacycline against USA300 and *mntC*::Tn
563 cultured in SWF and MHB. n = 6 from three independent experiments, shown as mean ± SEM.
564 Significant difference were determined between USA300 cultured in MHB and SWF for D, E, F
565 by Welch's t-test, and in G (I; USA300 and USA300 Dox), (II; *mntC*::Tn and *mntC*::Tn Dox) and
566 (III; *mntC*::Tn Dox and PBS) by Logrank (Mantel-Cox) test and (IV; *mntC*::Tn and USA300) at
567 day 1 by two-way ANOVA and the Tukey post hoc test. $p < 0.0001$ (****), $p < 0.001$ (***), $p$
568 $< 0.01$ (**), $p < 0.05$ (*).
569

570

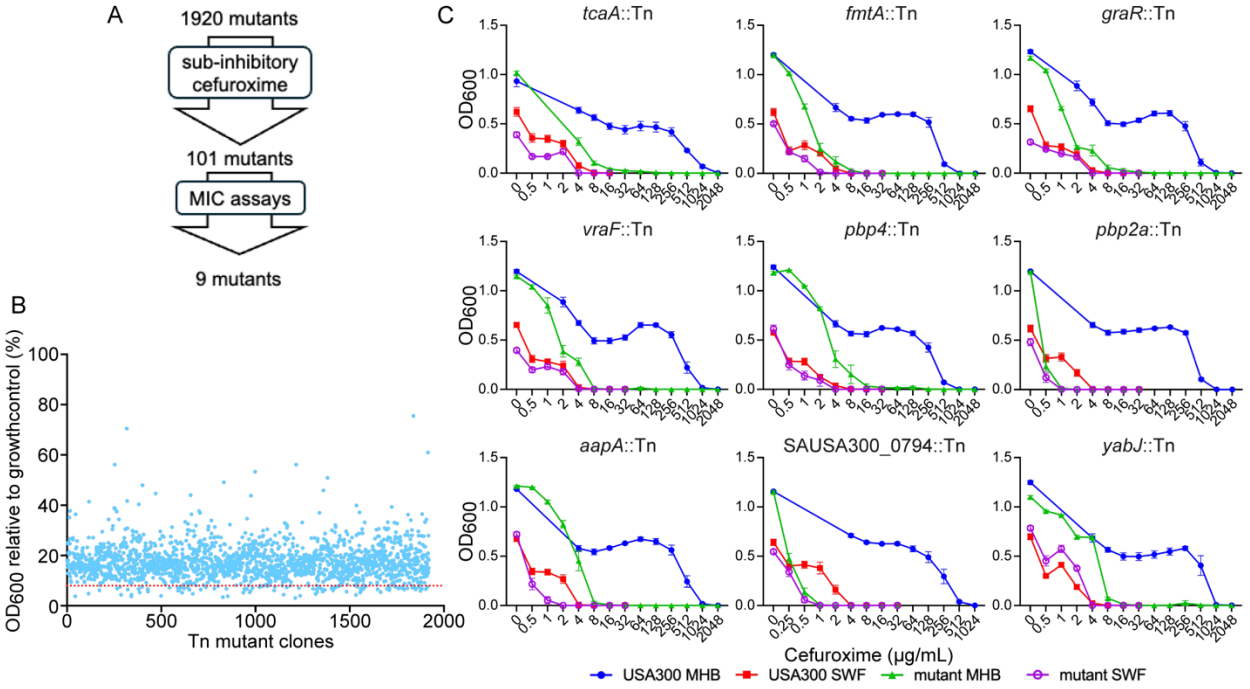


571

572 **Fig. 2 | A chemogenomic screen identifies putative determinants of USA300 sensitivity to**

573 **cefuroxime in SWF.**

574 A) The workflow of the chemogenomic screen and follow-up assays that led to the identification

575 of putative determinants of cefuroxime sensitivity. B) A chemogenomic screen of the Nebraska

576 Transposon Mutant Library with cefuroxime at 1/8$^{th}$ MIC of the wild-type strain in MHB. C)

577 MIC assays of putative determinants uncovered in the screen; n ≥ 6 from at least three

578 independent experiments shown as mean ± SEM.

579

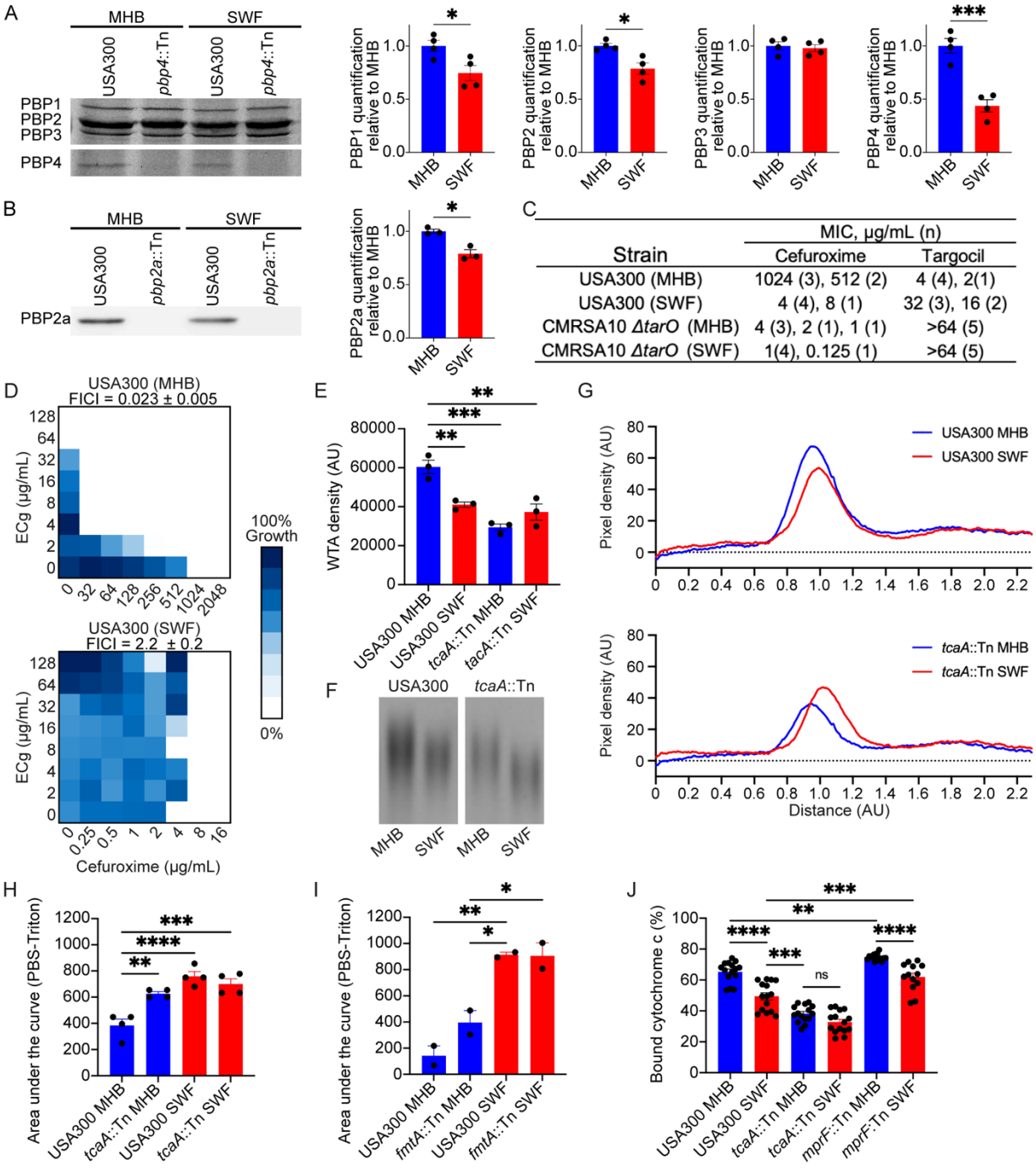


580

581 **Fig. 3 | Decrease in the abundance of PBPs and wall teichoic acid in SWF contributes to**

582 **USA300 cefuroxime sensitivity.**

583 A) Quantification of PBP1, 2, 3, 4 from USA300 cultured in SWF (red) relative to MHB (blue),

584 n = 4 from two independent membrane isolations, shown as mean ± SEM and one representative

585 BOCILLIN FL-labeled gel. All uncropped gels are shown in Fig. S9B) PBP2a quantification
586 from Western blots, using an anti-PBP2a antibody, of membranes isolated from USA300 cultured
587 in SWF (red) relative to MHB (blue), n = 3 from three independent membrane isolations, shown
588 as mean ± SEM and one representative blot. All uncropped blots are shown in Fig. S9C) MIC of
589 cefuroxime and targocil against USA300 or CMRSA10*ΔtarO* cultured in MHB or SWF, n = 5
590 biological replicates each performed in triplicate. D) Representative checkerboard assays of *S.*
591 *aureus* USA300 of cefuroxime in combination with epicatechin gallate (ECg). n = 5. FICI shown
592 as mean ± SEM. E) Relative quantity of PAGE-resolved crude WTA from *S. aureus* USA300 or
593 *tcaA*::Tn cultured in MHB or SWF. n = 3 shown as mean ± SEM. F) Representative PAGE gel
594 of WTA isolated from USA300 or *tcaA*::Tn cultured in MHB or SWF. Uncropped gel is shown in
595 Fig. S10G) Relative band migration of WTA on PAGE represented as mean pixel density. n = 3
596 from three independent WTA isolations. H-I) Area under the curve (AUC) of lysis rates
597 represented as PBS AUC – 0.02% Triton AUC comparing lysis rates of USA300 and *tcaA*::Tn
598 (H; n=4) and *fmtA*::Tn (I; n=2) cultured from MHB or SWF. Shown as mean ± SEM. Full lysis
599 curves and AUC calculation are shown in Fig. S10J) Percent cytochrome c binding to USA300
600 or mutants cultured in MHB or SWF, which infers relative cell charge. n = 15 or n = 13 for
601 *mprF*::Tn SWF from 5 independent experiments, shown as mean ± SEM. Significant differences
602 were determined by Welch's t-test (A and B) and one-way ANOVA and the Tukey post hoc test
603 (E, H, I, and J). $p < 0.0001$ (****), $p < 0.001$ (***), $p < 0.01$ (**), and $p < 0.05$ (*).
604

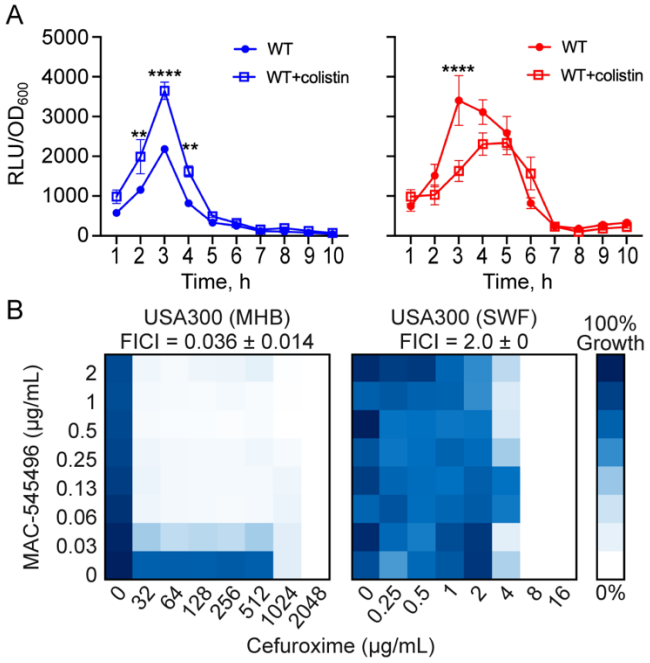


605

606 **Fig. 4 | Disruption of GraXSR VraFG in SWF contributes to cefuroxime sensitivity.**

607 A) Monitoring the luciferase expression under the control of the *mprF* promoter in USA300 over

608 10 h in TSB (Blue) or SWF (Red) in the presence or absence of 1/32 MIC of colistin. n = 4

609 shown as mean ± SEM. Significant differences were determined between the with and without

610 colistin conditions by two-way ANOVA and the Bonferroni post hoc test. $p < 0.0001$ (****), $p$

611 $< 0.001$ (***), $p < 0.01$ (**), $p < 0.05$ (*). B) Representative cefuroxime and MAC-545496

612 checkerboard assays against *S. aureus* USA300. Dark blue represents high cell density, measured

613 by $OD_{600}$, n = 3, FICI shown as mean ± SEM.

614

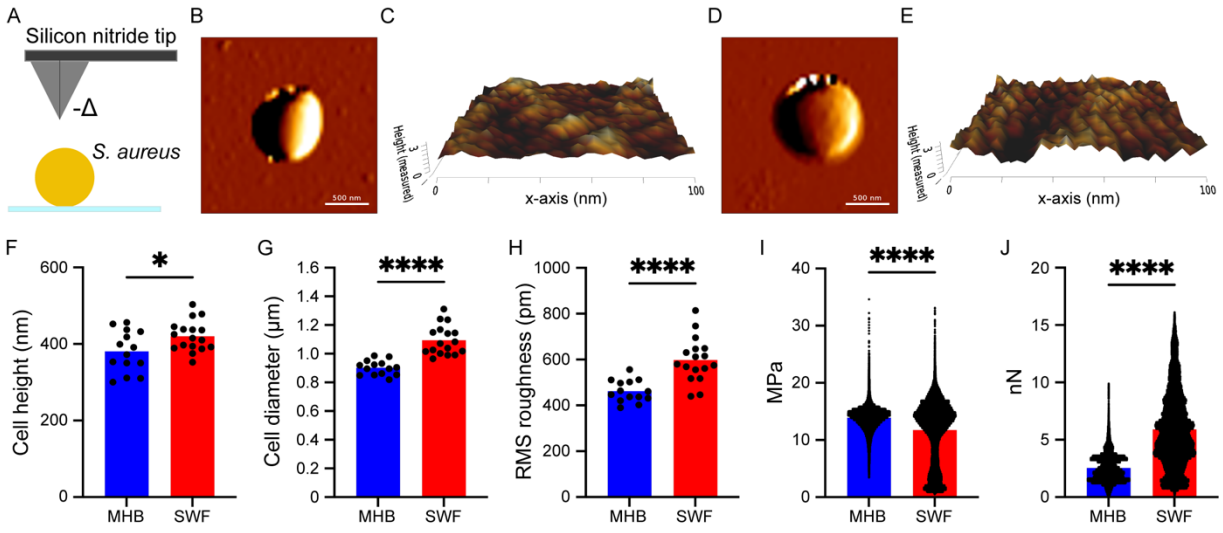


615

616 **Fig. 5 | Atomic force microscopy of USA300 cultured in MHB and SWF**

617 A) A schematic diagram of the AFM probe, B-E) Representative images (B, D) and 3D images of

618 cell surface topography (C, E) of USA300 cultured in MHB (B, C) and SWF (D, E). All AFM

619 images used for quantitative analyses are shown in Fig. S13 and S14F) Cell height of USA300

620 cultured in MHB and SWF. G) Cell diameter of USA300 cultured in MHB and SWF. H) Root

621 mean squared (RMS) roughness of the flattest 100 nm x 100 nm region from a 0.4 x 0.4 µm scan

622 area. I-J) Viscoelasticity and adhesion of USA300 cultured in MHB n = 91079 and SWF n =

623 118114. Significant differences between USA300 cultured in MHB and SWF were determined

624 by Welch's t-test. $p < 0.0001$ (****), $p < 0.001$ (***), $p < 0.01$ (**), $p < 0.05$ (*).

625

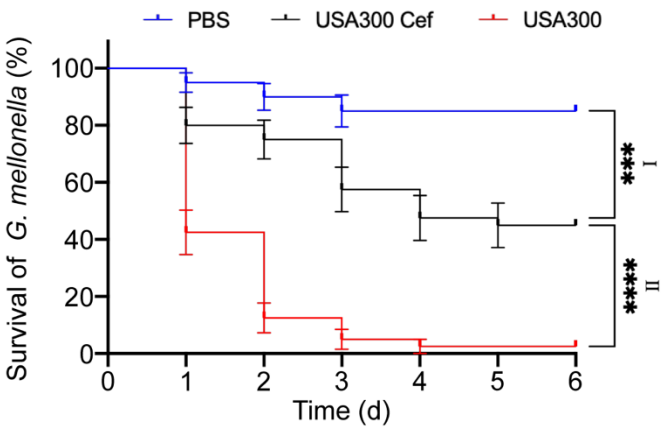


626

627 **Fig. 6 | Cefuroxime increases larval survival *in vivo Galleria* wound infection.**

628 Kaplan-Meier survival curve of larvae shown as mean ± SE. PBS with vehicle treatment (blue),

629 infection with USA300 and vehicle treatment (red), and infection with USA300 and cefuroxime

630 treatment (black), n = 40 from 4 independent experiments. Significant differences were

631 determined between (I; PBS and USA300 Cef) and (II; USA300 and USA300 Cef) by the

632 Logrank (Mantel-Cox) test. $p < 0.0001$ (****), $p < 0.001$ (***), $p < 0.01$ (**), $p < 0.05$ (*).

633

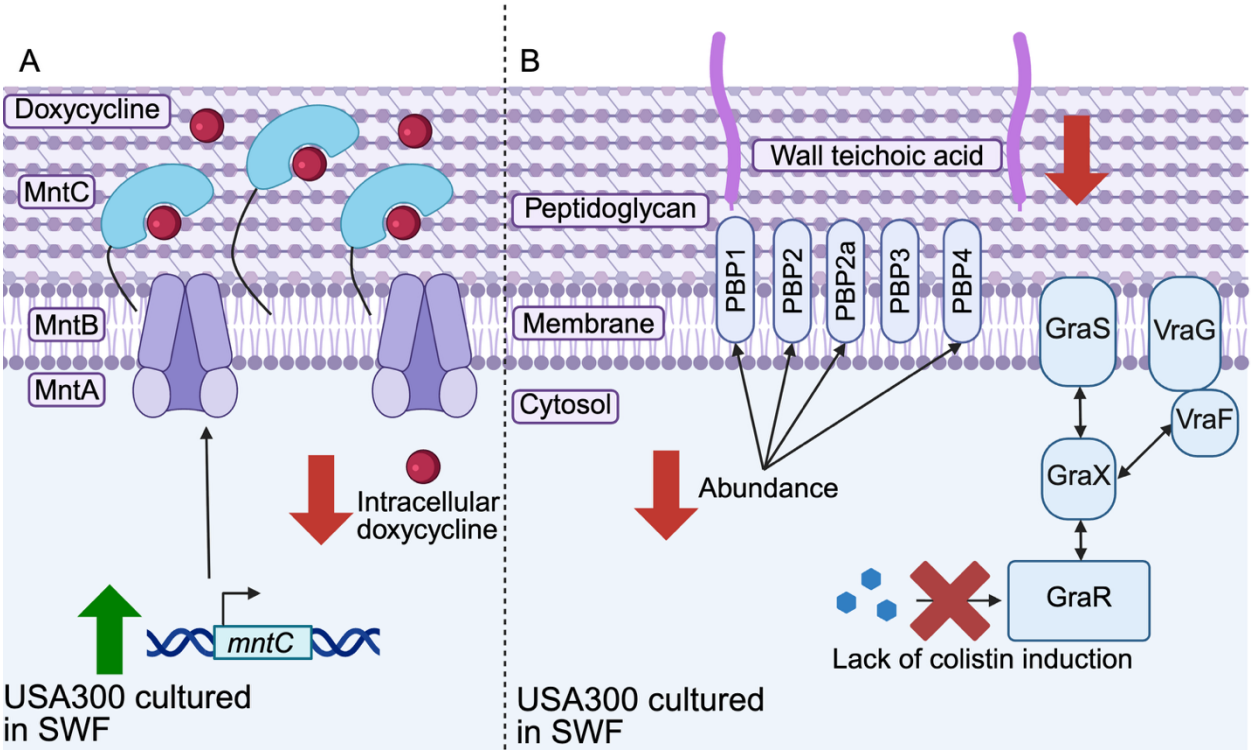


**Fig. 7 | Summary of mechanisms underlying the altered susceptibility of MRSA USA300 to tetracyclines and β-lactams under wound infection-like conditions.**

A) Summary of alterations in USA300 that led to increased resistance to tetracyclines when cultured in SWF, depicting an increase in expression of MntC, which binds to doxycycline (a tetracycline), reducing its intracellular concentration. B) Summary of cell envelope-related remodelling in USA300 that increased susceptibility to β-lactams when cultured in SWF, displaying decreased abundance of penicillin binding proteins PBP1, 2, 2a, 4 and wall teichoic acid, along with a lack of the antimicrobial peptide colistin-mediated GraXSR VraFG induction. Created using Biorender.

646 **Tables**

647 **Table 1. USA300 MIC assays conducted in SWF relative to those in MHB**
648 MICs from at least three independent experiments.

| Antibiotic class | Antibiotic | MIC, µg/mL | | Fold | CLSI breakpoint, µg/mL | | |
|---|---|---|---|---|---|---|---|
| | | MHB | SWF | shift* | R, ≥ | S, ≤ | Ref |
| Lipopeptides | Daptomycin | 4 | 1 | 4 ↓ | - | 1 | [91] |
| Fluoroquinolones | Ciprofloxacin | 32 | 16 | 2 ↓ | 4 | 1 | [91] |
| Glycopeptides | Vancomycin | 2 | 1 | 2 ↓ | 16 | 2 | [91] |
| Rifampins | Rifampicin | 0.008 | 0.064 | 8 ↑ | 4 | 1 | [91] |
| β-lactams | Cefuroxime | 1024 | 4 | 256 ↓ | 32 | 8 | [92] |
| | Oxacillin | 64 | 1 | 64 ↓ | 4 | 2 | [91] |
| Polymyxins | Colistin | 512 | 32 | 16 ↓ | | | |
| Tetracyclines | Tetracycline | 0.25 | 32 | 128 ↑ | 16 | 4 | [91] |
| | Doxycycline | 0.125 | 4 | 32 ↑ | 16 | 4 | [91] |
| | Omadacycline | 0.25 | 0.5 | 2 ↑ | | | |
| Macrolides | Azithromycin | 2 | 0.0156 | 128 ↓ | 8 | 2 | [91] |
| Aminoglycosides | Kanamycin | 4 | 4 | No shift | 64 | 16 | [18] |

649 * Fold increase or decrease in SWF relative to MHB.

650

651 **Table 2. MIC of cefuroxime, oxacillin, and doxycycline against isolates representing the**
652 **most commonly circulating lineages of MRSA in Canada.** MICs average of three independent
653 experiments.

| Strain | Lineage | MIC in MHB (µg/mL) | | | MIC in SWF (µg/mL) | | |
|---|---|---|---|---|---|---|---|
| | | cefuroxime | oxacillin | doxycycline | cefuroxime | oxacillin | doxycycline |
| CMRSA 1 | USA600 | >2048 | 1024 | 0.25 | >2048 | 1024 | 2 |
| CMRSA 2 | USA100/800 | >2048 | 512 | 0.25 | 16 | 32 | 4 |
| CMRSA 3 | | >2048 | 512 | 16 | 512 | 256 | >128 |
| CMRSA 4 | USA200 | 2048 | 256 | 0.25 | 2048 | 256 | 4 |
| CMRSA 5 | USA500 | 256 | 32 | 8 | 8 | 1 | >128 |
| CMRSA 6 | | >2048 | 512 | 16 | 1024 | 256 | >128 |
| CMRSA 7 | USA400/MW2 | 1024 | 64 | 0.25 | 8 | 2 | 2 |
| CMRSA 8 | EMRSA15 | 1024 | 64 | 0.25 | 4 | 8 | 2 |
| CMRSA 9 | | 2048 | 256 | 0.25 | 16 | 32 | 4 |
| CMRSA 10 | USA300 | 1024 | 64 | 0.25 | 4 | 2 | 4 |

654

655 **STAR methods:**

656 **Key resources table**

| REAGENT or RESOURCE | SOURCE | IDENTIFIER |
|---|---|---|
| Antibodies | | |
| Anti-Mouse IgG, peroxidase-linked species-specific whole antibody | Fisher Scientific | Cat#45000679 |
| *Staphylococcus aureus* PBP2a (Methicillin-resistant) Monoclonal antibody (AC10) | Thermo Fisher Scientific | Cat#MAC-46568; RRID: AB_2937640 |
| Bacterial and virus strains | | |
| Refer to Table S1 | This work | N/A |
| Chemicals, peptides, and recombinant proteins | | |
| Daptomycin | Cedarlane | TRC-D193350 |
| Ciprofloxacin | Sigma-Aldrich | Cat#17850 |
| Vancomycin | Sigma-Aldrich | Cat#V1130 |
| Rifampicin | Sigma-Aldrich | Cat#R7382 |
| Cefuroxime | Sigma-Aldrich | Cat#C4417 |
| Oxacillin | Sigma-Aldrich | Cat#28221 |
| Colistin | Sigma-Aldrich | Cat#C4461 |
| Tetracycline | Sigma-Aldrich | Cat#T7660 |
| Doxycycline | Fisher Scientific | Cat#D41165G |
| Omadacycline | Cayman Chemical Co. | Cat#24932 |
| Azithromycin | Sigma-Aldrich | Cat#PHR1088 |
| Kanamycin | Sigma-Aldrich | Cat#K1377 |
| Erythromycin | Sigma-Aldrich | Cat#E5389 |
| IPTG | Sigma-Aldrich | Cat#16758 |
| cOmplete™ protease inhibitor cocktail | Roche | Cat#11836170001 |
| His-select nickel-affinity gel | Sigma-Aldrich | Cat#P6611 |
| Bovine serum albumin | Sigma-Aldrich | Cat#10735078001 |
| Lysozyme | Sigma-Aldrich | Cat#L1667 |
| Triton X-100 | Fisher Scientific | Cat#BP151-100 |
| Cytochrome c | Sigma-Aldrich | Cat#C2506 |
| Proteinase K | Fisher Scientific | Cat#70-663-4 |
| BOCILLIN™ FL | Fisher Scientific | Cat#B13233 |
| Cell-Tak™ | Corning | Cat#354240 |
| Fetal bovine serum | Fisher Scientific | Cat#FB12999102 |
| MOPS | Fisher Scientific | Cat#BP308-100 |
| HEPES | Fisher Scientific | Cat#BP310-100 |
| Tris base | Fisher Scientific | Cat#BP152-500 |
| BBL™ Mueller Hinton II Broth (Cation-Adjusted) | Fisher Scientific | Cat#B12322 |
| BACTO™ Tryptic Soy Broth | Fisher Scientific | Cat#DF0370-17-3 |
| | | |
| Critical commercial assays | | |
| Bio-Rad Protein Assay Dye Reagent | Bio-Rad | Cat#5000006 |
| Monarch Total RNA | New England Biolabs | Cat#T2010S |
| TURBO DNA-free™ kit | Fisher Scientific | Cat#AM1907 |
| Superscript™ III First-Strand Synthesis | Fisher Scientific | Cat#18-080-051 |
| FastStart SYBR Green | Sigma-Aldrich | Cat#4673484001 |

| | | |
|---|---|---|
| 1-stepTM Ultra TMB-Blotting Solution | Fisher Scientific | Cat#P137574 |
| Blocker™ FL | Fisher Scientific | Cat#PI37565 |
| Monarch Spin PCR & DNA Cleanup kit | New England Biolabs | Cat#T1130L |
| Monarch Spin Plasmid Miniprep kit | New England Biolabs | Cat#T1110L |
| Oligonucleotides | | |
| Refer to Table S2 | This work | N/A |
| Recombinant DNA | | |
| Refer to Table S1 | This work | N/A |
| Software and algorithms | | |
| GraphPad Prism 10 | GraphPad | https://www.graphpad.com/ |
| ImageJ | ImageJ | https://imagej.net/ij/ |
| JPK SPM Data Processing v5.1 | Bruker | N/A |

657

658 **Strains and reagents.** Table S1 lists the strains and plasmids, and Table S2 lists the
659 primers used in this study. Bacteria were grown in cation-adjusted Mueller-Hinton broth (MHB)
660 or simulated wound fluid (50% Fetal bovine serum from Fisher Scientific, 50% Maximum
661 recovery diluent (MRD; 1g/L peptone, 8.5g/L NaCl) at 37 ºC, unless otherwise specified.

662

663 **Antimicrobial Susceptibility Testing (AST).** MICs were determined by broth
664 microdilution according to CLSI guidelines [93]. The assays were conducted in microtiter plates
665 with a final inoculum adjusted to an $OD_{600}$ of 0.001, prepared by the colony resuspension
666 method. The plates were then incubated at 37ºC with shaking, and bacterial growth was
667 determined by measuring the $OD_{600}$ after 24 h. When MIC values were not reached within the
668 tested concentration range, the highest tested concentration was considered half the MIC. The
669 fractional inhibitory concentration indices (FICI) were calculated as FICI = ($MIC_A$ in
670 combination/$MIC_A$ alone) + ($MIC_B$ in combination/$MIC_B$ alone). FICI values ≤0.5 were
671 interpreted as synergy, >0.5 to ≤4.0 as additive or indifferent, and >4.0 as antagonistic.

672

673 **Nebraska transposon mutant library (NTML) screen.** Overnight cultures of the
674 NTML [38] were prepared in 384-well plates using Biomatrix BM6-BC (S&P Robotics Inc.) in
675 MHB with 5 µg/mL erythromycin (Sigma-Aldrich). The following day, these overnight cultures
676 were used to inoculate MHB or SWF with or without doxycycline (Fisher Scientific) or
677 cefuroxime (Sigma-Aldrich), at the concentrations indicated in the results section, using the
678 BM6-BC. All 384-well plates were incubated at 37 ºC and 600 RPM, and the $OD_{600}$ was read
679 after 24 h.
680
681 **Dose-response assay.** Selected NTML strains were re-arrayed and inoculated into 96-
682 well plates in MHB containing 5 µg/mL erythromycin using the BM6-BC. The following day,
683 96-well plates with varying antibiotic concentrations in MHB and SWF were inoculated using
684 the BM6-BC. All plates were incubated at 37 ºC and 600 RPM, and the $OD_{600}$ was read after 24
685 h.
686
687 **Genetic complementation.** To complement *mntB*::Tn and *mntC*::Tn, PCR fragments
688 were amplified using USA300 gDNA as template and primer pairs (listed in Table S2):
689 mntB_compF3_AvrII and mntB_compR2_BamHI for *mntB*, mntB_compF3_AvrII and
690 mntC_compR_BamHI for *mntBC*, and mntC_compF3_AvrII and mntC_compR_BamHI for
691 *mntC*. Fragments and pKK22-Pfba were digested with AvrII and BamHI (New England Biolabs),
692 and the plasmid was alkaline phosphatase-treated (using Antarctic phosphatase, New England
693 Biolabs), followed by ligation with T4 DNA ligase (New England Biolabs) to generate the
694 complementation vectors, pKK22-Pfba-*mntB*, pKK22-Pfba-*mntBC*, and pKK22-Pfba-*mntC*.

695 Complementation and control vectors were transformed into electrocompetent *S. aureus* strains
696 by electroporation (Bio-Rad) [94].
697
698 **Doxycycline accumulation assay.** Cultures were started from a single colony and
699 incubated overnight in MHB or SWF at 37 ºC with shaking, then sub-cultured by diluting to an
700 $OD_{600}$ of 0.1 in fresh media and further incubated for 6 h. Cells were harvested from the sub-
701 cultures and resuspended at an $OD_{600}$ of 1 in MHB or SWF. Doxycycline was added to 1 mL of
702 these OD-adjusted cultures at a final concentration of 5 µg/mL, and the cultures were incubated
703 for 30 min at 37 ºC. Cells were pelleted, resuspended in 1 mL of fresh culture media, and
704 incubated for 15 min at 37 ºC. The cells were then washed twice with PBS and resuspended in
705 0.5 mL of PBS, followed by dispensing of 100 µL aliquots into 96-well black plates in
706 quintuplicate and read at $\lambda_{ex}$ = 400 nm / $\lambda_{em}$ = 530 nm. The bacterial suspensions were also
707 transferred to a clear 96-well plate for $OD_{600}$ measurement. All centrifugation steps were at 6,000
708 × g for 1 min.
709
710 **Protein overexpression and purification.** *mntC* was cloned into pET28a(+) and
711 transformed into $CaCl_2$ chemically competent *E. coli* BL21 by heat shock. Bacterial cultures
712 were incubated at 30 ºC and 250 RPM until an $OD_{600}$ of ~0.8 was reached, then induced with 0.5
713 mM IPTG and further incubated for 5 h at 30 ºC. Cells were harvested, resuspended in lysis
714 buffer [50 mM sodium phosphate, 500 mM NaCl, cOmplete™ protease inhibitor cocktail
715 (Roche), pH 8.0], and lysed using Lysing Matrix B (MP Biomedicals) and the FastPrep-24™.
716 The supernatants were separated from the insoluble fractions by centrifugation at 10,000 × g for
717 15 min at 4 ºC. His-tagged proteins were batch purified from the supernatants using His-select

718 nickel-affinity gel (Sigma-Aldrich), washed three times with wash buffer (50 mM sodium
719 phosphate, 500 mM NaCl, 5 mM imidazole, pH 8.0), and eluted with elution buffer (50 mM
720 sodium phosphate, 500 mM NaCl, 250 mM imidazole, pH 8.0), followed by detection on a 12%
721 acrylamide gel (Bio-Rad) stained with PageBlue™ (Fisher Scientific). The eluted protein was
722 dialyzed using 10 kDa SnakeSkin™ dialysis tubing (Fisher Scientific) into 20 mM HEPES, pH
723 7.4, 100 mM NaCl buffer, then quantified using the Bradford method with protein assay dye
724 reagent concentrate (Bio-Rad).
725
726 **Doxycycline binding assay.** Purified MntC, bovine serum albumin (BSA), and lysozyme
727 solutions in dialysis buffer (20 mM HEPES, pH 7.4, 100 mM NaCl) were each incubated at 37
728 ºC with doxycycline in the dark for 4 h at a final volume of 200 µL and final concentration of 32
729 µM of protein and 16 µM of doxycycline in 96-well black plates. Wells containing only 200 µL
730 of buffer with 16 µM of doxycycline and 200 µL of buffer with 32 µM of protein were used for
731 background subtraction of fluorescent signal. Plates were then read at $\lambda_{ex}$ = 390 nm / $\lambda_{em}$ = 550
732 nm.
733
734 **RNA extraction.** USA300 cultures were grown overnight and diluted to an $OD_{600}$ of 0.05
735 in MHB or SWF. Cells were grown at 37 ºC to an $OD_{600}$ of 0.6, then treated with doxycycline (8
736 µg/mL) or vehicle control (ultrapure water) for 30 minutes. Aliquots (6 mL) of the cultures were
737 collected, centrifuged at 3,320 × g for 10 min. RNA was extracted using Monarch Total RNA
738 miniprep (New England Biolabs), followed by treatment with Invitrogen Turbo DNA-free DNase
739 (Fisher Scientific) following the manufacturer's protocol. RNA purity was assessed by
740 measuring the ratio of absorbance at 260 nm to 280 nm (values obtained ~2.0).

741

742 **cDNA synthesis and RT-PCR.** RNA was converted to cDNA with Superscript™ III
743 First-Strand Synthesis System (Fisher Scientific) following the manufacturer's protocol. RT-PCR
744 was performed using the QuantStudio™ 5 Real-Time PCR (Thermo Fisher Scientific) with
745 FastStart SYBR Green (Roche). Fold change in gene expression was calculated using the Pfaffl
746 Method [95] relative to *arcC* and 16s rRNA.

747

748 ***Galleria mellonella* incision wound infection model.** *G. mellonella* larvae weighing
749 ~300 mg were selected, anesthetized by chilling at 4 ºC for 10 minutes, and kept on ice during
750 incision and treatment application. Incisions spanning the third segment from the posterior end of
751 the larvae were made parasagittally on the dorsal side. Larvae were inoculated with 2 µL of
752 inoculum (0.0001 $OD_{600}$/mg of larva weight). After 30 min, 4 µL of a 10% w/w doxycycline
753 compounded in Glaxal™ Base, 40% w/w cefuroxime compounded in Glaxal™ Base, or vehicle
754 control (water in Glaxal™ Base) was applied to the inoculated wounds. Worms were then
755 incubated at 37 ºC and monitored for survival for 6 days. Of note, research ethics approval is not
756 required for the use of this invertebrate model.

757

758 **Lysis Assay.** Overnight cultures were diluted to an $OD_{600}$ of 0.1 and grown to an $OD_{600}$ of
759 0.8. Cells were washed and resuspended in PBS or PBS containing 0.02% Triton X-100 (Fisher
760 Scientific) at a cell density of 1 OD/mL. The bacterial suspensions were dispensed into 200 µL
761 aliquots in triplicate in 96-well plates, incubated at 37 ºC with shaking in the plate reader, and
762 their $OD_{600}$ was read every 15 min for 6 h.

763

764 **Cytochrome c binding assay.** The assay was performed as previously described [96].
765 Briefly, overnight cultures were adjusted to an $OD_{600}$ of 1, and 8 mL were pelleted, washed twice
766 in MOPS buffer (20 mM, pH 7.0), and resuspended in a total volume of 200 µL MOPS. A 50 µL
767 aliquot of a 2.5 mg/mL cytochrome c solution (Sigma-Aldrich) was added to the 200 µL
768 resuspended culture and incubated at room temperature for 10 min. The samples were then
769 pelleted at 16,000 × g for 1 min, and 200 µL of the supernatants were dispensed into 96-well
770 plates, and their absorbance was read at 530 nm ($A_{530nm}$). *mprF*::Tn was used as a positive
771 control.
772
773 **Bioluminescence assay.** The luciferase expression assay was conducted as previously
774 described [58], except that bacteria were cultured in either TSB or SWF. Briefly, USA300
775 (pGYlux::*mprF*), USA300 (pGYlux::*ilvD*), Δ*graR* (pGYlux::*mprF*), and USA300 with control
776 vector pGYlux were grown overnight in TSB and SWF with 10 µg/mL chloramphenicol. The
777 overnight cultures were then diluted to an $OD_{600}$ of 0.01 in 10 mL of TSB or SWF with and
778 without 1/32$^{nd}$ MIC of colistin and grown at 37 ºC with shaking. Each hour, 100 µL was plated
779 into a white 96-well plate in triplicate, and relative light units (RLU) were measured before
780 transferring to a clear 96-well plate to measure $OD_{600}$.
781
782 **WTA isolation.** Crude WTA was isolated as previously described [97], with minor
783 modifications to normalize the quantity of bacteria prior to WTA isolation. Briefly, overnight
784 cultures in either MHB or SWF were washed once with buffer 1 (50 mM MES, pH 6.5) and
785 volumes corresponding to an $OD_{600}$ of 5 were centrifuged at 5,000 × g, resuspended in buffer 2
786 [4% (w/v) SDS, 50 mM MES, pH 6.5], and boiled for 1 h, followed by washing in buffer 1 and

787 transferring into 1.5 mL microcentrifuge tubes. Pellets were then washed with 1.4 mL of buffer
788 2, then with 1.4 mL of buffer 3 (2% NaCl, 50 mM MES, pH 6.5), followed by 1.4 mL of buffer 1
789 with all spins at 16,000 × g for 1 min. Pellets were resuspended in 1 mL of digestion buffer [20
790 mM Tris-HCl, pH 8.0, 0.5% (w/v) SDS] with the addition of 10 µL of 2 mg/mL proteinase K.
791 Samples were digested at 50 ºC for 4 h with shaking (1000 rpm). Pellets were then washed with
792 1.4 mL of buffer 3, followed by three 1.4 mL washes of ultrapure water. The pellets were then
793 resuspended in 1 mL of 0.1 M NaOH and incubated at 20 ºC for 16 h with shaking at 1000 rpm
794 in an infors HT Multitron incubator (3 mm throw diameter). The samples were then centrifuged
795 at 16,000 × g for 1 min, and 750 µL of the supernatants were transferred to a new
796 microcentrifuge tube. Subsequently, 250 µL of 1 M Tris-HCl, pH 7.8, was added to neutralize the
797 reaction.
798
799 **WTA PAGE.** Aliquots (15 µL) of crude WTA were mixed with 5 µL of 4x loading dye
800 (50% glycerol with bromophenol blue), and 10 µL was loaded and separated on tricine
801 polyacrylamide gels at 40 mA [97] until the dye front had reached the bottom of the gel. Gels were
802 washed three times with ultrapure water, then stained with Alcian Blue 8GX (Fisher Scientific, 1
803 mg/mL) overnight, and destained with ultrapure water until the bands became visible.
804
805 **Membrane preparation.** Cultures grown overnight at 37 ºC with shaking were diluted to
806 an $OD_{600}$ of 0.05 and then grown to an $OD_{600}$ of 0.8. The cultures were pelleted, resuspended in
807 PBS, and lysed using Lysing Matrix B (MP Biomedicals) and the FastPrep-24™. Cell debris was
808 pelleted at 10,000 × g for 30 min, and the supernatant was centrifuged at 40,000 rpm for 1h to

809 pellet the membrane, which was then resuspended in PBS, and its protein content was quantified
810 by the Bradford method using protein assay dye reagent concentrate (Bio-Rad).
811
812 **BOCILLIN™ FL assay.** Membrane fractions (equivalent to 30 µg of protein content)
813 from USA300 and *pbp4*::Tn cultured in MHB and SWF were incubated with 20 µM of
814 BOCILLIN™ FL (Fisher Scientific) at 37 ºC for 10 min, followed by the addition of 4x Laemmli
815 buffer and boiling for 5 min. Membrane samples were resolved on 10% SDS-PAGE running at
816 80V for 30 min, followed by 120V for 2.25 h. Gels were then visualized using the Typhoon FLA
817 7000 gel scanner (GE Healthcare), and the band intensities were subsequently quantified with
818 ImageJ. PBP quantifications were background-subtracted by membrane-free BOCILLIN™ FL
819 lanes.
820
821 **PBP2a western blot.** Membrane fractions (equivalent to 10 µg of protein content) from
822 USA300 and *pbp2a*::Tn cultured in MHB and SWF were resolved on 10% SDS-PAGE, running
823 at 80 V for 30 min, followed by 120 V for 2.25 h. Protein bands were transferred to
824 nitrocellulose film using a Mini Trans-Blot® Cell (Bio-Rad) at 100 V for 2 h. The nitrocellulose
825 membrane was then blocked overnight at 4 ºC with Blocker™ FL (Thermo Scientific). The
826 primary antibody, mouse anti-*S. aureus*-PBP2a (Thermo Fisher Scientific) (1:1000 dilution in
827 Blocker™ FL), was incubated for 2 h at room temperature with rocking. The secondary antibody,
828 a horseradish peroxidase-conjugated sheep anti-Mouse IgG (Thermo Scientific) (1:1000 dilution
829 in Blocker™ FL buffer), was incubated for 2 h at room temperature with rocking. The blot was
830 developed with 1-Step™ Ultra TMB-Blotting Solution (Thermo Scientific) for 10 min, then

831 visualized on the Gel Doc™ EZ imager (Bio-Rad), and band intensities were subsequently
832 quantified with ImageJ.
833
834 **Atomic force microscopy (AFM) imaging.** AFM (Nanowizard 4; JPK Instruments,
835 Berlin, Germany) in quantitative imaging (QI™) mode [98,99] was used to analyze cell surface
836 topography and mechanics of USA300 cells cultured in MHB and SWF. Overnight cultures of
837 USA300 in MHB and SWF were diluted to an $OD_{600}$ of 0.05 and grown to an $OD_{600}$ of 0.6. Cells
838 were then washed three times in PBS and resuspended to an $OD_{600}$ of 0.125 and deposited onto
839 clean, Cell-Tak™ (Corning®)-coated coverslips [100], incubated for 30 min at room temperature
840 followed by rinsing with ultrapure water three times, air dried (30 min) at room temperature, and
841 imaged using non-conductive silicon nitride cantilevers (Multi-cantilever Tip (MLCT), D
842 cantilever, nominal k = 0.03 N/m and tip radius 20 nm; Bruker, USA). Cantilever spring constant
843 (0.028 N/m) was calibrated using the thermal noise method [101]. QI™ force curves at each pixel
844 of a 128 × 128 raster scan were collected using a Z-length of 1000 nm, setpoint of 2 nN, and a
845 raster scan of 100 µm/s, along with a subset of force curves within a 0.4 × 0.4 nm square in the
846 center of the cell. Force curves were batch-processed using JPK SPM Data Processing software
847 (version 5.1, JPK, Berlin, Germany), and histogram data were exported to Excel.
848
849 **Statistical analysis.** All statistical analyses were calculated using GraphPad Prism 10. The
850 statistical test used for each assay is indicated in the figure captions.
851
852

## References


1. Laxminarayan, R., Duse, A., Wattal, C., Zaidi, A.K., Wertheim, H.F., Sumpradit, N., Vlieghe, E., Hara, G.L., Gould, I.M., Goossens, H., et al. (2013). Antibiotic resistance-the need for global solutions. Lancet Infect Dis *13*, 1057–1098. 10.1016/S1473-3099(13)70318-9.
2. Ibberson, C.B., and Whiteley, M. (2020). The social life of microbes in chronic infection. Current opinion in microbiology *53*, 44–50. 10.1016/j.mib.2020.02.003.
3. Lazarus, G.S., Cooper, D.M., Knighton, D.R., Percoraro, R.E., Rodeheaver, G., and Robson, M.C. (1994). Definitions and guidelines for assessment of wounds and evaluation of healing. Wound Repair Regen *2*, 165–170. 10.1046/j.1524-475X.1994.20305.x.
4. Schultz, G.S., Chin, G.A., Moldawer, L., and Diegelmann, R.F. (2011). Principles of Wound Healing. In Mechanisms of Vascular Disease: A Reference Book for Vascular Specialists, R. Fitridge, and M. Thompson, eds.
5. Cutting, K.F. (2003). Wound exudate: composition and functions. Br J Community Nurs *8*, suppl 4–9. 10.12968/bjcn.2003.8.sup3.11577.
6. Falanga, V., Isseroff, R.R., Soulika, A.M., Romanelli, M., Margolis, D., Kapp, S., Granick, M., and Harding, K. (2022). Chronic wounds. Nat Rev Dis Primers *8*, 50. 10.1038/s41572-022-00377-3.
7. Queen, D., and Harding, K. (2023). What's the true costs of wounds faced by different healthcare systems around the world? International Wound Journal *20*, 3935–3938. https://doi.org/10.1111/iwj.14491.
8. Queen, D., and Harding, K. (2024). Estimating the cost of wounds both nationally and regionally within the top 10 highest spenders. Int Wound J *21*, e14709. 10.1111/iwj.14709.
9. Rahim, K., Saleha, S., Zhu, X.D., Huo, L., Basit, A., and Franco, O.L. (2017). Bacterial Contribution in Chronicity of Wounds. Microb Ecol *73*, 710–721. 10.1007/s00248-016-0867-9.
10. Murray, C.J., Ikuta, K.S., Sharara, F., Swetschinski, L., Aguilar, G.R., Gray, A., Han, C., Bisignano, C., Rao, P., and Wool, E. (2022). Global burden of bacterial antimicrobial resistance in 2019: a systematic analysis. The lancet *399*, 629–655.
11. Tong, S.Y.C., Davis, J.S., Eichenberger, E., Holland, T.L., and Fowler, V.G. (2015). *Staphylococcus aureus* Infections: Epidemiology, Pathophysiology, Clinical Manifestations, and Management. Clinical Microbiology Reviews *28*, 603–661. 10.1128/Cmr.00134-14.
12. Norbury, W., Herndon, D.N., Tanksley, J., Jeschke, M.G., Finnerty, C.C., and Infection, S.S.C.S. (2016). Infection in Burns. Surg Infect *17*, 250–255. 10.1089/sur.2013.134.
13. Gjødsbøl, K., Christensen, J.J., Karlsmark, T., Jørgensen, B., Klein, B.M., and Krogfelt, K.A. (2006). Multiple bacterial species reside in chronic wounds: a longitudinal study. Int Wound J *3*, 225–231. 10.1111/j.1742-481X.2006.00159.x.
14. Pastagia, M., Kleinman, L.C., Lacerda de la Cruz, E.G., and Jenkins, S.G. (2012). Predicting risk for death from MRSA bacteremia. Emerg Infect Dis *18*, 1072–1080. 10.3201/eid1807.101371.
15. WHO (2017). Prioritization of pathogens to guide discovery, research and development of new antibiotics for drug-resistant bacterial infections including tuberculosis. World Health Organization.

16. Nichol, K.A., Adam, H.J., Golding, G.R., Lagace-Wiens, P.R.S., Karlowsky, J.A., Hoban, D.J., Zhanel, G.G., Canadian Antimicrobial Resistance, A., and Canward (2019). Characterization of MRSA in Canada from 2007 to 2016. J Antimicrob Chemother *74*, iv55–iv63. 10.1093/jac/dkz288.
17. Mueller, J.H., and Hinton, J. (1941). A protein-free medium for primary isolation of the Gonococcus and Meningococcus. Proc. Soc. Expt. Biol. Med. *48*, 330–333. https://doi.org/10.3181/00379727-48-13311.
18. CLSI. (2017). Performance Standards for Antimicrobial Susceptibility Testing; 27th Edition. CLSI supplement M100. (Clinical and Laboratory Standards Institute).
19. Macgowan, A.P., and Surveillance, B.W.P.o.R. (2008). Clinical implications of antimicrobial resistance for therapy. J Antimicrob Chemother *62 Suppl 2*, ii105–114. 10.1093/jac/dkn357.
20. Hurley, M.N., Ariff, A.H., Bertenshaw, C., Bhatt, J., and Smyth, A.R. (2012). Results of antibiotic susceptibility testing do not influence clinical outcome in children with cystic fibrosis. J Cyst Fibros *11*, 288–292. 10.1016/j.jcf.2012.02.006.
21. Smith, A.L., Fiel, S.B., Mayer-Hamblett, N., Ramsey, B., and Burns, J.L. (2003). Susceptibility testing of *Pseudomonas aeruginosa* isolates and clinical response to parenteral antibiotic administration: lack of association in cystic fibrosis. Chest *123*, 1495–1502.
22. Tong, M., French, S., El Zahed, S.S., Ong, W.K., Karp, P.D., and Brown, E.D. (2020). Gene Dispensability in *Escherichia coli* Grown in Thirty Different Carbon Environments. mBio *11*. 10.1128/mBio.02259-20.
23. Zlitni, S., Ferruccio, L.F., and Brown, E.D. (2013). Metabolic suppression identifies new antibacterial inhibitors under nutrient limitation. Nat Chem Biol *9*, 796–804. 10.1038/nchembio.1361.
24. Bowler, P.G., Jones, S.A., Walker, M., and Parsons, D. (2004). Microbicidal properties of a silver-containing hydrofiber dressing against a variety of burn wound pathogens. J Burn Care Rehabil *25*, 192–196. 00004630-200403000-00009 [pii].
25. Wound exudate and the role of dressings. A consensus document. (2008). Int Wound J *5 Suppl 1*, iii–12. 10.1111/j.1742-481X.2008.00439.x.
26. Aiba-Kojima, E., Tsuno, N.H., Inoue, K., Matsumoto, D., Shigeura, T., Sato, T., Suga, H., Kato, H., Nagase, T., Gonda, K., et al. (2007). Characterization of wound drainage fluids as a source of soluble factors associated with wound healing: comparison with platelet-rich plasma and potential use in cell culture. Wound Repair Regen *15*, 511–520. 10.1111/j.1524-475X.2007.00259.x.
27. Iizaka, S., Sanada, H., Minematsu, T., Oba, M., Nakagami, G., Koyanagi, H., Nagase, T., Konya, C., and Sugama, J. (2010). Do nutritional markers in wound fluid reflect pressure ulcer status? Wound Repair Regen *18*, 31–37. 10.1111/j.1524-475X.2009.00564.x.
28. James, T.J., Hughes, M.A., Cherry, G.W., and Taylor, R.P. (2000). Simple biochemical markers to assess chronic wounds. Wound Repair Regen *8*, 264–269. 10.1046/j.1524-475x.2000.00264.x.
29. Trengove, N.J., Langton, S.R., and Stacey, M.C. (1996). Biochemical analysis of wound fluid from nonhealing and healing chronic leg ulcers. Wound Repair Regen *4*, 234–239. 10.1046/j.1524-475X.1996.40211.x.
30. Lee, D.Y., Lee, S.Y., Yun, S.H., Jeong, J.W., Kim, J.H., Kim, H.W., Choi, J.S., Kim, G.D., Joo, S.T., Choi, I., and Hur, S.J. (2022). Review of the Current Research on Fetal Bovine

Serum and the Development of Cultured Meat. Food Sci Anim Resour *42*, 775–799. 10.5851/kosfa.2022.e46.

31. Slade, E.A., Thorn, R.M.S., Young, A., and Reynolds, D.M. (2019). An *in vitro* collagen perfusion wound biofilm model; with applications for antimicrobial studies and microbial metabolomics. BMC Microbiol *19*, 310. 10.1186/s12866-019-1682-5.
32. Rowley, A.F., and Ratcliffe, N.A. (1978). A histological study of wound healing and hemocyte function in the wax-moth *Galleria mellonella*. J Morphol *157*, 181–199. 10.1002/jmor.1051570206.
33. Maslova, E., Shi, Y., Sjoberg, F., Azevedo, H.S., Wareham, D.W., and McCarthy, R.R. (2020). An Invertebrate Burn Wound Model That Recapitulates the Hallmarks of Burn Trauma and Infection Seen in Mammalian Models. Front Microbiol *11*, 998. 10.3389/fmicb.2020.00998.
34. Nelson, M.L., and Levy, S.B. (2011). The history of the tetracyclines. Ann Ny Acad Sci *1241*, 17–32. 10.1111/j.1749-6632.2011.06354.x.
35. Brown, N.M., Goodman, A.L., Horner, C., Jenkins, A., and Brown, E.M. (2021). Treatment of methicillin-resistant *Staphylococcus aureus* (MRSA): updated guidelines from the UK. JAC Antimicrob Resist *3*, dlaa114. 10.1093/jacamr/dlaa114.
36. Farha, M.A., Leung, A., Sewell, E.W., D'Elia, M.A., Allison, S.E., Ejim, L., Pereira, P.M., Pinho, M.G., Wright, G.D., and Brown, E.D. (2013). Inhibition of WTA Synthesis Blocks the Cooperative Action of PBPs and Sensitizes MRSA to beta-Lactams. Acs Chem Biol *8*, 226–233. 10.1021/cb300413m.
37. Christianson, S., Golding, G.R., Campbell, J., and Mulvey, M.R. (2007). Comparative genomics of Canadian epidemic lineages of methicillin-resistant *Staphylococcus aureus*. J Clin Microbiol *45*, 1904–1911. 10.1128/Jcm.02500-06.
38. Fey, P.D., Endres, J.L., Yajjala, V.K., Widhelm, T.J., Boissy, R.J., Bose, J.L., and Bayles, K.W. (2013). A genetic resource for rapid and comprehensive phenotype screening of nonessential *Staphylococcus aureus* genes. MBio *4*, e00537–00512. 10.1128/mBio.00537-12.
39. Horsburgh, M.J., Wharton, S.J., Cox, A.G., Ingham, E., Peacock, S., and Foster, S.J. (2002). MntR modulates expression of the PerR regulon and superoxide resistance in *Staphylococcus aureus* through control of manganese uptake. Mol Microbiol *44*, 1269–1286. 10.1046/j.1365-2958.2002.02944.x.
40. Tan, X., Song, Z., and Wang, Z. (2016). Characterization of the interaction between bovine serum albumin and doxycycline by chemiluminescence and molecular docking. Instrumentation Science & Technology *44*, 294–307. 10.1080/10739149.2015.1105817.
41. Ramarao, N., Nielsen-Leroux, C., and Lereclus, D. (2012). The insect *Galleria mellonella* as a powerful infection model to investigate bacterial pathogenesis. J Vis Exp, e4392. 10.3791/4392.
42. Glavis-Bloom, J., Muhammed, M., and Mylonakis, E. (2012). Of model hosts and man: using *Caenorhabditis elegans*, *Drosophila melanogaster* and *Galleria mellonella* as model hosts for infectious disease research. Advances in experimental medicine and biology *710*, 11–17. 10.1007/978-1-4419-5638-5_2.
43. Douglas, E.J.A., Palk, N., Brignoli, T., Altwiley, D., Boura, M., Laabei, M., Recker, M., Cheung, G.Y.C., Liu, R., Hsieh, R.C., et al. (2023). Extensive re-modelling of the cell wall during the development of *Staphylococcus aureus* bacteraemia. eLife. 10.7554/elife.87026.2.

44. Rahman, M.M., Hunter, H.N., Prova, S., Verma, V., Qamar, A., and Golemi-Kotra, D. (2016). The *Staphylococcus aureus* Methicillin Resistance Factor FmtA Is a d-Amino Esterase That Acts on Teichoic Acids. mBio *7*, e02070–02015. 10.1128/mBio.02070-15.
45. Hartman, B.J., and Tomasz, A. (1984). Low-affinity penicillin-binding protein associated with beta-lactam resistance in *Staphylococcus aureus*. J Bacteriol *158*, 513–516. 10.1128/jb.158.2.513-516.1984.
46. Reed, P., Atilano, M.L., Alves, R., Hoiczyk, E., Sher, X., Reichmann, N.T., Pereira, P.M., Roemer, T., Filipe, S.R., Pereira-Leal, J.B., et al. (2015). *Staphylococcus aureus* Survives with a Minimal Peptidoglycan Synthesis Machine but Sacrifices Virulence and Antibiotic Resistance. PLoS Pathog *11*, e1004891. 10.1371/journal.ppat.1004891.
47. Falord, M., Karimova, G., Hiron, A., and Msadek, T. (2012). GraXSR Proteins Interact with the VraFG ABC Transporter To Form a Five-Component System Required for Cationic Antimicrobial Peptide Sensing and Resistance in *Staphylococcus aureus*. Antimicrob Agents Ch *56*, 1047–1058. 10.1128/Aac.05054-11.
48. Huang, Y.-H., Yeh, W.-B., Chang, R., Chen, C.-Y., Wing-Yan Chan, M., Chou, M.-C., and Chen, C.-C. (2025). A novel $\sigma^B$ regulatory module in *Staphylococcus aureus:* Unraveling the multifaceted roles of RsbU domains in stress response mechanisms. Journal of Microbiology, Immunology and Infection. https://doi.org/10.1016/j.jmii.2025.05.007.
49. Fuchs, S., Mehlan, H., Bernhardt, J., Hennig, A., Michalik, S., Surmann, K., Pané-Farré, J., Giese, A., Weiss, S., Backert, L., et al. (2018). AureoWiki‑The repository of the *Staphylococcus aureus* research and annotation community. International Journal of Medical Microbiology *308*, 558–568. https://doi.org/10.1016/j.ijmm.2017.11.011.
50. Mlynek, K.D., Callahan, M.T., Shimkevitch, A.V., Farmer, J.T., Endres, J.L., Marchand, M., Bayles, K.W., Horswill, A.R., and Kaplan, J.B. (2016). Effects of Low-Dose Amoxicillin on *Staphylococcus aureus* USA300 Biofilms. Antimicrob Agents Chemother *60*, 2639–2651. 10.1128/AAC.02070-15.
51. Maria, J.P.S., Sadaka, A., Moussa, S.H., Brown, S., Zhang, Y.J., Rubin, E.J., Gilmore, M.S., and Walker, S. (2014). Compound-gene interaction mapping reveals distinct roles for *Staphylococcus aureus* teichoic acids. P Natl Acad Sci USA *111*, 12510–12515. 10.1073/pnas.1404099111.
52. Lee, A.S., de Lencastre, H., Garau, J., Kluytmans, J., Malhotra-Kumar, S., Peschel, A., and Harbarth, S. (2018). Methicillin-resistant *Staphylococcus aureus*. Nature Reviews Disease Primers *4*. ARTN 18033
10.1038/nrdp.2018.33.
53. Hamilton, S.M., Alexander, J.A.N., Choo, E.J., Basuino, L., da Costa, T.M., Severin, A., Chung, M., Aedo, S., Strynadka, N.C.J., Tomasz, A., et al. (2017). High-Level Resistance of *Staphylococcus aureus* to beta-Lactam Antibiotics Mediated by Penicillin-Binding Protein 4 (PBP4). Antimicrob Agents Chemother *61*. 10.1128/AAC.02727-16.
54. Sewell, E.W.C., and Brown, E.D. (2014). Taking aim at wall teichoic acid synthesis: new biology and new leads for antibiotics. Journal of Antibiotics *67*, 43–51. 10.1038/ja.2013.100.
55. Campbell, J., Singh, A.K., Maria, J.P.S., Kim, Y., Brown, S., Swoboda, J.G., Mylonakis, E., Wilkinson, B.J., and Walker, S. (2011). Synthetic Lethal Compound Combinations Reveal a Fundamental Connection between Wall Teichoic Acid and Peptidoglycan Biosyntheses in *Staphylococcus aureus*. Acs Chemical Biology *6*, 106–116. 10.1021/cb100269f.

1037 56. D'Elia, M.A., Henderson, J.A., Beveridge, T.J., Heinrichs, D.E., and Brown, E.D. (2009).
1038 The *N*-Acetylmannosamine Transferase Catalyzes the First Committed Step of Teichoic
1039 Acid Assembly in *Bacillus subtilis* and *Staphylococcus aureus*. J Bacteriol *191*, 4030–
1040 4034. 10.1128/Jb.00611-08.
1041 57. Lee, K., Campbell, J., Swoboda, J.G., Cuny, G.D., and Walker, S. (2010). Development
1042 of improved inhibitors of wall teichoic acid biosynthesis with potent activity against
1043 *Staphylococcus aureus*. Bioorg Med Chem Lett *20*, 1767–1770.
1044 10.1016/j.bmcl.2010.01.036.
1045 58. El-Halfawy, O.M., Czarny, T.L., Flannagan, R.S., Day, J., Bozelli, J.C., Jr., Kuiack, R.C.,
1046 Salim, A., Eckert, P., Epand, R.M., McGavin, M.J., et al. (2020). Discovery of an
1047 antivirulence compound that reverses beta-lactam resistance in MRSA. Nat Chem Biol
1048 *16*, 143–149. 10.1038/s41589-019-0401-8.
1049 59. Lu, Y., Chen, F., Zhao, Q., Cao, Q., Chen, R., Pan, H., Wang, Y., Huang, H., Huang, R.,
1050 Liu, Q., et al. (2023). Modulation of MRSA virulence gene expression by the wall
1051 teichoic acid enzyme TarO. Nat Commun *14*, 1594. 10.1038/s41467-023-37310-5.
1052 60. Komatsuzawa, H., Sugai, M., Ohta, K., Fujiwara, T., Nakashima, S., Suzuki, J., Lee,
1053 C.Y., and Suginaka, H. (1997). Cloning and characterization of the *fmt* gene which affects
1054 the methicillin resistance level and autolysis in the presence of triton X-100 in
1055 methicillin-resistant *Staphylococcus aureus*. Antimicrob Agents Ch *41*, 2355–2361. Doi
1056 10.1128/Aac.41.11.2355.
1057 61. Xia, G., Kohler, T., and Peschel, A. (2010). The wall teichoic acid and lipoteichoic acid
1058 polymers of *Staphylococcus aureus*. Int J Med Microbiol *300*, 148–154.
1059 10.1016/j.ijmm.2009.10.001.
1060 62. Slavetinsky, C.J., Hauser, J.N., Gekeler, C., Slavetinsky, J., Geyer, A., Kraus, A.,
1061 Heilingbrunner, D., Wagner, S., Tesar, M., Krismer, B., et al. (2022). Sensitizing
1062 *Staphylococcus aureus* to antibacterial agents by decoding and blocking the lipid flippase
1063 MprF. Elife *11*. 10.7554/eLife.66376.
1064 63. Falord, M., Mader, U., Hiron, A., Debarbouille, M., and Msadek, T. (2011). Investigation
1065 of the *Staphylococcus aureus* GraSR regulon reveals novel links to virulence, stress
1066 response and cell wall signal transduction pathways. PLoS One *6*, e21323.
1067 10.1371/journal.pone.0021323.
1068 64. Farha, M.A., Tu, M.M., and Brown, E.D. (2025). Important challenges to finding new
1069 leads for new antibiotics. Current opinion in microbiology *83*. ARTN 102562
1070 10.1016/j.mib.2024.102562.
1071 65. van Belkum, A., Bachmann, T.T., Ludke, G., Lisby, J.G., Kahlmeter, G., Mohess, A.,
1072 Becker, K., Hays, J.P., Woodford, N., Mitsakakis, K., et al. (2019). Developmental
1073 roadmap for antimicrobial susceptibility testing systems. Nat Rev Microbiol *17*, 51–62.
1074 10.1038/s41579-018-0098-9.
1075 66. Ledger, E.V.K., Mesnage, S., and Edwards, A.M. (2022). Human serum triggers
1076 antibiotic tolerance in *Staphylococcus aureus*. Nat Commun *13*, 2041. 10.1038/s41467-
1077 022-29717-3.
1078 67. Somerville, G.A., Parrett, A.A., Reed, J.M., Gardner, S.G., Morton, M., and Powers, R.
1079 (2022). Human Serum Alters the Metabolism and Antibiotic Susceptibility of
1080 *Staphylococcus aureus*. J Proteome Res *21*, 1467–1474. 10.1021/acs.jproteome.2c00073.
1081 68. Weber, B., De Jong, A., Guo, A., Dharavath, S., French, S., Fiebig-Comyn, A., Coombes,
1082 B., Magolan, J., and Brown, E. (2020). Genetic and Chemical Screening in Human Blood

1083 Serum Reveals Unique Antibacterial Targets and Compounds against *Klebsiella*
1084 *pneumoniae*. Cell reports *32 3*, 107927. 10.1016/j.celrep.2020.107927.
1085 69. Di Bonaventura, G., Lupetti, V., Di Giulio, A., Muzzi, M., Piccirilli, A., Cariani, L., and
1086 Pompilio, A. (2023). Repurposing High-Throughput Screening Identifies Unconventional
1087 Drugs with Antibacterial and Antibiofilm Activities against *Pseudomonas aeruginosa*
1088 under Experimental Conditions Relevant to Cystic Fibrosis. Microbiol Spectr *11*,
1089 e0035223. 10.1128/spectrum.00352-23.
1090 70. Carfrae, L.A., MacNair, C.R., Brown, C.M., Tsai, C.N., Weber, B.S., Zlitni, S., Rao, V.N.,
1091 Chun, J., Junop, M.S., Coombes, B.K., and Brown, E.D. (2020). Mimicking the human
1092 environment in mice reveals that inhibiting biotin biosynthesis is effective against
1093 antibiotic-resistant pathogens. Nat Microbiol *5*, 93–101. 10.1038/s41564-019-0595-2.
1094 71. Ersoy, S.C., Heithoff, D.M., Barnes, L.t., Tripp, G.K., House, J.K., Marth, J.D., Smith,
1095 J.W., and Mahan, M.J. (2017). Correcting a Fundamental Flaw in the Paradigm for
1096 Antimicrobial Susceptibility Testing. EBioMedicine *20*, 173–181.
1097 10.1016/j.ebiom.2017.05.026.
1098 72. Heithoff, D.M., Barnes, V.L., Mahan, S.P., Fried, J.C., Fitzgibbons, L.N., House, J.K.,
1099 and Mahan, M.J. (2023). Re-evaluation of FDA-approved antibiotics with increased
1100 diagnostic accuracy for assessment of antimicrobial resistance. Cell Rep Med *4*, 101023.
1101 10.1016/j.xcrm.2023.101023.
1102 73. Jin, S., Lim, S.Y., Lee, Y.W., Sung, H., Kim, M.-N., Bae, S., Jung, J., Kim, M.J., Kim, S.-
1103 H., Lee, S.-O., et al. (2025). Clinical and microbiological analysis of risk factors for
1104 breakthrough bloodstream infection during Tigecycline Therapy. Scientific Reports *15*,
1105 4266. 10.1038/s41598-025-88048-7.
1106 74. Parsonage, M., Shah, S., Moss, P., Thaker, H., Meigh, R., Balaji, A., Elston, J., and
1107 Barlow, G. (2010). Breakthrough bacteraemia with a susceptible *Enterococcus faecalis*
1108 during tigecycline monotherapy. J Antimicrob Chemother *65*, 370–374.
1109 10.1093/jac/dkp455.
1110 75. Anderson, A.S., Miller, A.A., Donald, R.G., Scully, I.L., Nanra, J.S., Cooper, D., and
1111 Jansen, K.U. (2012). Development of a multicomponent *Staphylococcus aureus* vaccine
1112 designed to counter multiple bacterial virulence factors. Hum Vaccin Immunother *8*,
1113 1585–1594. 10.4161/hv.21872.
1114 76. Anderson, A.S., Scully, I.L., Timofeyeva, Y., Murphy, E., McNeil, L.K., Mininni, T.,
1115 Nuñez, L., Carriere, M., Singer, C., Dilts, D.A., and Jansen, K.U. (2012). *Staphylococcus*
1116 *aureus* Manganese Transport Protein C Is a Highly Conserved Cell Surface Protein That
1117 Elicits Protective Immunity Against *S. aureus* and *Staphylococcus epidermidis*. The
1118 Journal of Infectious Diseases *205*, 1688–1696. 10.1093/infdis/jis272.
1119 77. Chaves-Moreno, D., Wos-Oxley, M.L., Jauregui, R., Medina, E., Oxley, A.P., and Pieper,
1120 D.H. (2016). Exploring the transcriptome of *Staphylococcus aureus* in its natural niche.
1121 Sci Rep *6*, 33174. 10.1038/srep33174.
1122 78. Moffitt, K., Cheung, E., Yeung, T., Stamoulis, C., and Malley, R. (2021). Analysis of
1123 *Staphylococcus aureus* Transcriptome in Pediatric Soft Tissue Abscesses and Comparison
1124 to Murine Infections. Infection and Immunity *89*. ARTN e00715-20
1125 10.1128/IAI.00715-20.
1126 79. Handke, L.D., Gribenko, A.V., Timofeyeva, Y., Scully, I.L., and Anderson, A.S. (2018).
1127 MntC-Dependent Manganese Transport Is Essential for *Staphylococcus aureus* Oxidative
1128 Stress Resistance and Virulence. mSphere *3*. 10.1128/mSphere.00336-18.

80. Elliott, D.J., Zaoutis, T.E., Troxel, A.B., Loh, A., and Keren, R. (2009). Empiric antimicrobial therapy for pediatric skin and soft-tissue infections in the era of methicillin-resistant *Staphylococcus aureus*. Pediatrics *123*, e959–966. 10.1542/peds.2008-2428.
81. Dhand, A., Bayer, A.S., Pogliano, J., Yang, S.-J., Bolaris, M., Nizet, V., Wang, G., and Sakoulas, G. (2011). Use of Antistaphylococcal β-Lactams to Increase Daptomycin Activity in Eradicating Persistent Bacteremia Due to Methicillin-Resistant *Staphylococcus aureus*: Role of Enhanced Daptomycin Binding. Clinical Infectious Diseases *53*, 158–163. 10.1093/cid/cir340.
82. Barber, K.E., Ireland, C.E., Bukavyn, N., and Rybak, M.J. (2014). Observation of "seesaw effect" with vancomycin, teicoplanin, daptomycin and ceftaroline in 150 unique MRSA strains. Infect Dis Ther *3*, 35–43. 10.1007/s40121-014-0023-0.
83. Casapao, A.M., Jacobs, D.M., Bowers, D.R., Beyda, N.D., and Dilworth, T.J. (2017). Early Administration of Adjuvant β-Lactam Therapy in Combination with Vancomycin among Patients with Methicillin-Resistant *Staphylococcus aureus* Bloodstream Infection: A Retrospective, Multicenter Analysis. Pharmacotherapy *37*, 1347–1356. 10.1002/phar.2034.
84. Truong, J., Veillette, J.J., and Forland, S.C. (2018). Outcomes of Vancomycin plus a β-Lactam versus Vancomycin Only for Treatment of Methicillin-Resistant *Staphylococcus aureus* Bacteremia. Antimicrob Agents Ch *62*. ARTN e01554-17 10.1128/AAC.01554-17.
85. Bush, K., and Bradford, P.A. (2016). β-Lactams and β-Lactamase Inhibitors: An Overview. Csh Perspect Med *6*. ARTN a025247 10.1101/cshperspect.a025247.
86. Rieger, C.D., Soliman, A.M., Kaplia, K., Ghosh, N., Lopez Alexa, C., Venkatesan Surya, A., Guevara Flores Abraham, G., Filiol Belin Matheus, A., Allen, F., Reynolds, M., et al. (2024). The antimicrobial potential of traditional remedies of Indigenous peoples from Canada against MRSA planktonic and biofilm bacteria in wound infection mimetic conditions. Microbiology Spectrum *12*, e02341–02324. 10.1128/spectrum.02341-24.
87. Demidova-Rice, T.N., Hamblin, M.R., and Herman, I.M. (2012). Acute and impaired wound healing: pathophysiology and current methods for drug delivery, part 1: normal and chronic wounds: biology, causes, and approaches to care. Adv Skin Wound Care *25*, 304–314. 10.1097/01.ASW.0000416006.55218.d0.
88. Svensby, A.U., Nygren, E., Gefen, A., Cullen, B., Ronkvist Å, M., Gergely, A., and Craig, M.D. (2024). The importance of the simulated wound fluid composition and properties in the determination of the fluid handling performance of wound dressings. Int Wound J *21*, e14861. 10.1111/iwj.14861.
89. Kadam, S., Madhusoodhanan, V., Dhekane, R., Bhide, D., Ugale, R., Tikhole, U., and Kaushik, K.S. (2021). Milieu matters: An *in vitro* wound milieu to recapitulate key features of, and probe new insights into, mixed-species bacterial biofilms. Biofilm *3*, 100047. 10.1016/j.bioflm.2021.100047.
90. Salazar, N., Castiblanco-Valencia, M.M., da Silva, L.B., de Castro, Í., Monaris, D., Masuda, H.P., Barbosa, A.S., and Arêas, A.P. (2014). *Staphylococcus aureus* manganese transport protein C (MntC) is an extracellular matrix- and plasminogen-binding protein. PLoS One *9*, e112730. 10.1371/journal.pone.0112730.
91. CLSI (2023). Performance Standards for Antimicrobial Susceptibility Testing CLSI supplement M100. Approved Standard, Pennsylvania *33rd ed*.

92. CLSI (2009). Performance Standards for Antimicrobial Susceptibility Testing CLSI supplement M100. Approved Standard, Pennsylvania *19th ed*.
93. CLSI (2012). Methods for dilution antimicrobial susceptibility tests for bacteria that grow aerobically. Approved Standard, Pennsylvania, 19087–11898.
94. Grosser, M.R., and Richardson, A.R. (2016). Method for Preparation and Electroporation of *S. aureus* and *S. epidermidis*. Methods Mol Biol *1373*, 51–57. 10.1007/7651_2014_183.
95. Pfaffl, M.W. (2001). A new mathematical model for relative quantification in real-time RT-PCR. Nucleic Acids Res *29*, e45.
96. Douglas, E.J.A., Alkhzem, A.H., Wonfor, T., Li, S.X., Woodman, T.J., Blagbrough, I.S., and Laabei, M. (2022). Antibacterial activity of novel linear polyamines against *Staphylococcus aureus*. Frontiers in Microbiology *13*. ARTN 948343 10.3389/fmicb.2022.948343.
97. Kho, K., and Meredith, T.C. (2018). Extraction and Analysis of Bacterial Teichoic Acids. Bio Protoc *8*, e3078. 10.21769/BioProtoc.3078.
98. Chopinet, L., Formosa, C., Rols, M.P., Duval, R.E., and Dague, E. (2013). Imaging living cells surface and quantifying its properties at high resolution using AFM in QI™ mode. Micron *48*, 26–33. 10.1016/j.micron.2013.02.003.
99. Bhat, S.V., Booth, S.C., Vantomme, E.A.N., Afroj, S., Yost, C.K., and Dahms, T.E.S. (2015). Oxidative stress and metabolic perturbations in *Escherichia coli* exposed to sublethal levels of 2,4-dichlorophenoxyacetic acid. Chemosphere *135*, 453–461. https://doi.org/10.1016/j.chemosphere.2014.12.035.
100. Shahina, Z., Bhat, S.V., Ndlovu, E., Sultana, T., Körnig, A., Dague, É., and Dahms, T.E. (2022). Cellulomics of Live Yeast by Advanced and Correlative Microscopy. In Laboratory Protocols in Fungal Biology: Current Methods in Fungal Biology, (Springer), pp. 159–174.
101. Lübbe, J., Temmen, M., Rahe, P., Kühnle, A., and Reichling, M. (2013). Determining cantilever stiffness from thermal noise. Beilstein J Nanotech *4*, 227–233. 10.3762/bjnano.4.23.